Unique alcohol dehydrogenases involved in algal sugar utilization by marine bacteria

Stefan Brott, Ki Hyun Nam, François Thomas, Theresa Dutschei, Lukas Reisky, Maike Behrens, Hanna Grimm, Gurvan Michel, Thomas Schweder, Uwe Bornscheuer

Unique alcohol dehydrogenases involved in algal sugar utilization by marine bacteria

Stefan Brott[1], Ki Hyun Nam[2], François Thomas[3], Theresa Dutschei[1], Lukas Reisky[1], Maike Behrens[1], Hanna C. Grimm[1], Gurvan Michel[3], Thomas Schweder[4], and Uwe T. Bornscheuer[1]*

[1]Department of Biotechnology & Enzyme Catalysis, Institute of Biochemistry, University of Greifswald, Greifswald 17487, Germany

[2]Department of Life Science, Pohang University of Science and Technology, Pohang 37673, South Korea

[3]Laboratory of Integrative Biology of Marine Models (LBI2M), Station Biologique de Roscoff (SBR), Sorbonne Université, CNRS 29688 Roscoff, Bretagne, France

[4]Department of Pharmaceutical Biotechnology, Institute of Pharmacy, University of Greifswald, Greifswald 17487, Germany

*Corresponding author: E-mail: uwe.bornscheuer@uni-greifswald.de

ORCID-IDs:

Stefan Brott: 0000-0003-2346-7706

Ki Hyun Nam: 0000-0003-3268-354X

François Thomas: 0000-0003-1896-0774

Theresa Dutschei: 0000-0003-3053-9536

Lukas Reisky: 0000-0001-8957-4083

Maike Behrens: 0000-0003-3757-588X

Hanna C. Grimm: 0000-0001-6352-0212

Gurvan Michel: 0000-0002-3009-6205

Thomas Schweder: 0000-0002-7213-3596

Uwe T. Bornscheuer: 0000-0003-0685-2696

Abstract

Marine algae produce complex polysaccharides, which can be degraded by marine heterotrophic bacteria utilizing carbohydrate-active enzymes. The red algal polysaccharide porphyran contains the methoxy sugar 6-*O*-methyl-D-galactose (G6Me). In the degradation of porphyran, an oxidative demethylation of this monosaccharide towards D-galactose and formaldehyde occurs, which is catalyzed by a cytochrome P450 monooxygenase and its redox partners. In direct proximity to the genes encoding for the key enzymes of this oxidative demethylation, genes encoding for zinc-dependent alcohol dehydrogenases (ADHs) were identified, which seem to be conserved in porphyran utilizing marine *Flavobacteriia*. Considering the fact that dehydrogenases could play an auxiliary role in carbohydrate degradation we aimed to elucidate the physiological role of these marine ADHs. Although, our results reveal that the ADHs are not involved in formaldehyde detoxification, a knockout of the ADH gene causes a dramatic growth defect of *Zobellia galactanivorans* with G6Me as substrate. This indicates that the ADH is required for G6Me utilization. Complete biochemical characterizations of the ADHs from *F. agariphila* KMM 3901^T (FoADH) and *Z. galactanivorans* Dsij^T (ZoADH) were performed and the substrate screening revealed that these enzymes preferentially convert aromatic aldehydes. Additionally, we elucidated the crystal structures of FoADH and ZoADH in complex with NAD^+ and show that the strict substrate specificity of these new auxiliary enzymes is based on a narrow active site.

Key points

- Knockout of the ADH encoding gene revealed its role in 6-*O*-methyl-D-galactose utilization, suggesting a new auxiliary activity in marine carbohydrate degradation
- Complete enzyme characterization indicated no function in a subsequent reaction of the oxidative demethylation such as formaldehyde detoxification
- These marine ADHs preferentially convert aromatic compounds and their strict substrate specificity is based on a narrow active site

Keywords

Alcohol dehydrogenase · Porphyran · CAZyme · Bacteroidetes · *Zobellia galactanivorans* · Auxiliary activity

Introduction

Marine algae represent one of the most crucial primary producers within the marine carbon cycle and contribute to approximately 50% of the total global primary production (Field 1998). For instance, macroalgae sequester approximately 173 Tg of carbon dioxide per year (Krause-Jensen and Duarte 2016) and accumulate the excess carbon in form of carbohydrates, which they utilize as cell wall constituents or energy storage (Arnosti et al. 2021). Degradation of these marine polysaccharides can be extremely complicated due their complexity and the occurrence of side chain modifications like sulfatations, methylations or acetylations (Bäumgen et al. 2021a). It was shown that complex enzymatic cascades are required for the breakdown of a single algal polysaccharide (Reisky et al. 2019; Sichert et al. 2020). Members of the bacterial phylum *Bacteroidetes* are considered specialists in the pivotal degradation of marine polysaccharides (Thomas et al. 2011a) and are observed as first responders after micro- and macroalgal blooms (Teeling et al. 2012; Brunet et al. 2021). They contain specific gene clusters referred to as polysaccharide utilization loci (PULs) (Grondin et al. 2017), which encode for carbohydrate-active enzymes (CAZymes) that catalyze the breakdown of the carbohydrates (Lapébie et al. 2019) as well as proteins essential for the binding and uptake of smaller sugar molecules (Bauer et al. 2006; Martens et al. 2009). Characterizing individual CAZymes helps elucidating complete degradation pathways of marine carbohydrates and provides a deeper understanding of the global carbon cycle. Which has been successfully performed for instance for ulvan from green algae (Reisky et al. 2019; Bäumgen et al. 2021b), fucoidan from brown algae (Sichert et al. 2020) and carrageenan from red algae (Ficko-Blean et al. 2017).

Recently, we have demonstrated that in the degradation process of the red algal galactan porphyran (Fig. 1a) by marine bacteria, an oxidative demethylation of the methoxy sugar 6-*O*-methyl-D-galactose (G6Me) occurs (Reisky et al. 2018). This reaction which is catalyzed by a cytochrome P450 monooxygenase (CYP) and its respective redox partners consisting of ferredoxin reductase and ferredoxin leads to the formation of equimolar amounts of D-galactose and formaldehyde (Fig. 1b) (Reisky et al. 2018). It was hypothesized that this reaction is crucial in terms of G6Me utilization, as it removes the highly stable methyl ether, consequently generating an easily metabolizable compound (Reisky et al. 2018). The crystal structure of the CYP from *Zobellia galactanivorans* Dsij^T provided additional information on the binding of G6Me as well as other mechanistic insights (Robb et al. 2018). In addition to the key enzymes for the oxidative demethylation of G6Me, glycoside hydrolases (GH2 and GH16), an esterase and a putative zinc-dependent alcohol dehydrogenase (ADH) were also observed in the genomic context of the marine *Flavobacteriia Formosa agariphila* KMM 3901^T (Fig. 1c) (Reisky et al. 2018). A similar genomic context was also found in *Zobellia galactanivorans* Dsij^T (Fig. 1d).

Considering the fact that dehydrogenases play only a minor auxiliary role in the carbohydrate degradation and are poorly represented in the Carbohydrate-Active enZYmes (CAZy) database, with some exceptions in the AA3, AA6, AA7 and AA12 families (Takeda et al. 2015; Kracher and Ludwig 2016; Sützl et al. 2018), it remains unclear which biological function this ADH provides for the organism. ADHs belong to the enzyme class of oxidoreductases and catalyze the reversible oxidation of an alcohol to the corresponding aldehyde or ketone employing the nicotinamide adenine dinucleotide (NAD^+) or nicotinamide adenine dinucleotide phosphate ($NADP^+$) cofactor. Depending on the size of the substrate-binding domain, it is possible for ADHs to possess a broad substrate scope; while some exhibit only activities for small aliphatic alcohols, others can convert sterically challenging cyclic components (Persson et al. 2008; Sirota et al. 2021). A major family of ADHs includes the group of zinc-dependent ADHs, which exhibit a typical Rossmann fold (Rao and Rossmann 1973) and contain a catalytic zinc in the active site as well as an additional non-catalytic zinc supporting the stability of an external loop structure (Hambidge et al. 2000). Various biological functions are observed within this family (Sirota et al. 2021) including polyol dehydrogenases catalyzing the conversion between sugar and sugar alcohol (Lu et al. 2019), cinnamyl alcohol dehydrogenases (Larroy et al. 2002; Pick et al. 2013) and glutathione-dependent formaldehyde dehydrogenases (Gutheil et al. 1992; Sanghani et al. 2000; Achkor et al. 2003) which play an important part in the detoxification of formaldehyde (Vorholt 2002). Additionally, ADHs provide numerous advantageous properties for organic synthesis including high enantioselectivity and applicability under mild reaction conditions (Koesoema et al. 2020). Consequently, they are now employed in numerous biotechnological applications such as the preparation of chiral alcohols (Zhang et al. 2015), rare sugars (Lu et al. 2019), fine chemicals as well as the synthesis of building blocks for various essential pharmaceuticals (Hall and Bommarius 2011; Zheng et al. 2017). Discovering and characterizing additional ADHs with unique biochemical properties, is thus also desirable for potential industrial applications.

In this study, we aimed to elucidated the putative function of these ADHs, which are consistently located in close proximity to genes that are essential for the oxidative demethylation of G6Me of polysaccharide utilizing marine *Flavobacteriia*. We provide a detailed biochemical characterization as well as the crystal structures for the ADHs from *Formosa agariphila* KMM 3901^T (FoADH) and *Zobellia galactanivorans* Dsij^T (ZoADH). We propose the putative biological functions of these ADHs and demonstrate their importance for the utilization of G6Me via growth studies with a *Z. galactanivorans* knockout strain.

Materials and Methods

Materials, strains and plasmids

All chemicals and reagents used, unless otherwise specified, were purchased from Sigma-Aldrich (St. Louis, MO, USA), Thermo Fisher Scientific (Waltham, MA, USA), Th. Geyer (Berlin, Germany), ABCR GmbH (Karlsruhe, Germany), Honeywell Fluka™ (Morristown, NJ, USA), Carl Roth GmbH (Karlsruhe, Germany), chemPUR GmbH (Karlsruhe, Germany), TCI Deutschland GmbH (Eschborn, Germany) and Cayman Chemical Company (Ann Arbor, MI, USA). Porphyran and G6Me were obtained from Biosynth Carbosynth (Staad, Switzerland). Primers were obtained from Invitrogen (Waltham, MA, USA). Phage-resistant *Escherichia coli* (*E. coli*) BL21 (genotype: *fhuA2* [lon] *ompT gal* (λ *DE3*) [*dcm*] Δ*hsdS* [λ *DE3* = λ *sBamHIo* Δ*Eco*RI-B int::(*lacI*::*PlacUV5*::*T7 gene1*) *i21* Δ*nin5*) was obtained from New England Biolabs (Ipswich, MA, USA). The conjugative strain *E. coli* S17-1 λ pir (genotype *λpir hsdR pro thi*; chromosomal integrated RP4-2 Tc::Mu Km::Tn7) (de Lorenzo and Timmis 1994) was grown from in-house glycerol stocks. A construct for the expression of the FoADH (GenBank accession number: OP548117) from *F. agariphila* KMM 3901^T was prepared using the FastCloning strategy (Li et al. 2011) with genomic DNA as template for the amplification of the insert. *F. agariphila* KMM 3901^T (collection number DSM-15362) was obtained from the DSMZ (Braunschweig, Germany). The pET28a vector was amplified with the 5-GCG GCC GCA CTC GAG CA-3′ and 5-CAT ATG GCT GCC GCG C-3’ oligonucleotides while the insert was amplified with the 5’-CAC AGC AGC GGC CTG GTG CCG CGC GGC AGC CAT ATG TCC ATA ATT TCA AAA TGC GCT ATT G-3′ and 5’-CAG TGG TGG TGG TGG TGG TGC TCG AGT GCG GCC GCT TAA AAA ATA ATT ACA CCC TTT GCA TTC-3’ oligonucleotides. A synthetic gene, codon optimized for expression in *E. coli*, encoding the ZoADH (GenBank accession number: OP548118) from *Z. galactanivorans* Dsij^T, was synthesized and cloned into a pET28a vector by BioCat GmbH (Heidelberg, Germany). The constructs encoded the recombinant protein as fusion to a N-terminal Strep-tag for affinity purification.

Computational analysis for FoADH and ZoADH

Sequences of FoADH (Uniprot ID: T2KM87) and ZoADH (Uniprot ID: G0L712) were blasted against the MarDB and MarRef database using the Marine Metagenomic Portal (Klemetsen et al. 2018; Priyam et al. 2019) with the -e value of $1e^{-5}$ and maximal target sequences of 1000. The automated fasta hit table of both blasts were fused and used for the generation of a sequence similarity network (Zallot et al. 2019). An alignment score of 150 was chosen for the refinement and generation of a genome neighborhood analysis of ten genes down and

upstream of the ADHs genes (Zallot et al. 2019). Resulting diagrams were visualized via Cytoscape (Paul Shannon et al. 2003) and genome neighborhood diagrams were generated from the online server. Only shared sequences of the MarDB/MarRef database with the UniProtKB databases could be incorporated in the genome neighborhood analysis.

ADH knockout in *Z. galactanivorans* and growth studies

The deletion mutant of the ADH gene *zgal_4674* in *Z. galactanivorans* Dsij^T (collection number DSM-12802) was constructed using a *sacB* system (Zhu et al. 2017) as previously described for the deletion variant of the CYP gene (Brott et al. 2022). Briefly, to delete *zgal_4674*, a 2,448 bp fragment including the last 43 bp of *zgal_4674* and 2,405 bp of downstream sequence was amplified using primers OFT0041 and OFT0043 on genomic DNA from *Z. galactanivorans* Dsij^T. The fragment was digested with BamHI and XbaI and ligated into pYT313 that had been digested with the same enzymes, to generate pFT12. A 2,077 bp fragment including the first 29 bp of *zgal_4674* and 2,048 bp of upstream sequence was amplified using primers OFT0040 and OFT0042. The fragment was cloned into XbaI and SalI sites of pFT12 to generate the *zgal_4674* deletion construct pFT13. Conjugative transfer of pFT13 from *E. coli* S17-1 into the wild-type *Z. galactanivorans* Dsij^T and second recombination steps were carried out as described previously (Zhu et al. 2017). Deletions were confirmed by PCR and sequencing on isolated colonies using primer pairs OFT0044- OFT0045 to identify the *zgal_4674* deletion mutant (mZG_0080). Primers employed are displayed in Table S1 in the Supplementary Information (SI). For growth studies, precultures of three *Z. galactanivorans* strains (wild type, knockout ADH and knockout CYP) were prepared in Zobell 2216E medium (Zobell 1941). The 3-day precultures were then rinsed twice with sterile saline solution. Marine minimal medium (Thomas et al. 2011a) amended with D-galactose or G6Me (4 g L^{-1}) was then inoculated so that an initial optical density (OD_{600}) of 0.05 was achieved. Appropriate cultures were incubated for 3 days at room temperature.

Enzyme production and purification

Chemically competent *E. coli* BL21 (DE3) cells were transformed with the plasmids harboring FoADH or ZoADH and were spread on lysogeny broth (LB) agar plates containing 50 µg mL^{-1} kanamycin. The agar plates were incubated overnight at 37 °C. One colony was picked and used to inoculate 5 mL LB medium which contained 50 µg mL^{-1} kanamycin and was then incubated at 37 °C and 180 rpm overnight. For overexpression the cultivation was performed in terrific broth (TB) medium containing 50 µg mL^{-1} kanamycin. The TB medium was inoculated with the overnight culture so that a starting OD_{600} of 0.05 was obtained. Cells were then incubated at 37 °C and 180 rpm until an OD_{600} of 0.8 was reached. Expression of target enzymes was induced by the addition of 1 mM isopropyl-β-D-thiogalactopyranoside (IPTG).

The cultivation was performed at 25 °C and 180 rpm overnight. Cells were harvested by centrifugation at 10,000 x *g* and 4 °C for 1 h, washed with 50 mM sodium phosphate buffer (NaPi) pH 7.5, and subsequently stored at -20 °C until cell disruption. The purification procedures of FoADH and ZoADH for crystallization and enzyme assays are identical. Cells were resuspended in 50 mM Tris-HCl buffer pH 8.0 containing 200 mM NaCl. Following cell lysis by ultra-sonication (2 × 3 min, 50% power, 50% cycle), cell debris was removed by centrifugation at 10,000 x *g*, at 4 °C for 20 min. The clarified supernatant was loaded on a gravity flow column containing Strep-Tactin XT Sepharose® 50% suspension (IBA-Lifesciences GmbH, Göttingen, Germany) as column material. The column was washed with 100 mM Tris-HCl buffer pH 8.0 containing 150 mM NaCl in order to remove unbound and undesirable proteins. The target enzymes were then eluted with same buffer containing additionally 50 mM biotin. Elution fractions were pooled and concentrated using a Vivaspin 6 centrifugal concentrator with a 10 kDa molecular weight cut-off (Sartorius AG, Göttingen, Germany). Size exclusion chromatography was subsequently performed via the Äkta™ pure chromatography system (Cytiva Europe GmbH, Germany). The concentrated enzyme solution was applied to a HiPrep™ 16/60 Sephacryl® S-200 HR column (Cytiva Europe GmbH, Freiburg, Germany) that was previously equilibrated with 10 mM Tris-HCl buffer pH 8.0 containing 200 mM NaCl. Elution fractions were collected and the purity was verified by sodium dodecyl sulfate-polyacrylamide gel electrophoresis (SDS-PAGE). Pure fractions were combined and concentrated like mentioned above. The enzyme solution was stored at 4 °C for crystallization. For application in enzyme assays, a PD-10 desalting column (Cytiva Europe GmbH, Freiburg, Germany) was employed to desalt the protein sample and exchange the buffer.

SDS-PAGE and determination of protein content

SDS-PAGE was performed to verify the purity of the target enzymes. 20 µL protein sample was mixed with 5 µL of a 5-fold stock of SDS sample buffer (100 mM Tris-HCl buffer pH 6.8 containing 4% (w/v) SDS, 20% (v/v) glycerol, 2% (v/v) β-mercaptoethanol, 25 mM ethylenediaminetetraacetic acid (EDTA) and 0.04% (w/v) bromophenol blue) and denatured at 99 ˚C for 15 min. For the SDS-PAGE a 12.5% acrylamide gel (separating gel) and a 4.0% loading gel were used. Electrophoresis was carried out at 200 V. Proteins were stained with Coomassie Blue (PhastGel® Blue R). As reference the Pierce™ Unstained protein molecular weight marker (Thermo Fisher Scientific, Waltham, MA, USA) was used. Protein concentrations were determined using the Pierce™ BCA Protein Assay Kit (Thermo Fisher Scientific, Waltham, MA, USA) with bovine serum albumin as protein standard.

Crystallization

Purified FoADH (25 mg mL^{-1}) and ZoADH (25 mg mL^{-1}) were incubated with 20 mM NAD^+ overnight. Initial crystallization screen was performed using sitting drop vapor-diffusion method at 22 °C. The droplets contained 0.2 µL of protein and 0.2 µL of reservoir solution. Microcrystals of FoADH were obtained from reservoir solution containing 0.1 M Tris-HCl pH 7.5, 0.2 M KCl and 22% (w/v) polyethylene glycol 3350. Microcrystals of ZoADH were obtained from reservoir solution containing 0.1 M Tris-HCl pH 7.5, 0.2 M KCl and 20% (w/v) polyethylene glycol 3350. Further crystal optimization was performed by scale-up of the droplets containing 2 µL of protein and 2 µL of reservoir solution, using the hanging drop vapor-diffusion method at 22 °C. Suitable FoADH and ZoADH crystals for X-ray diffraction were obtained from 0.1 M Tris-HCl, pH 7.5, 0.2 M KCl and 20-22% (w/v) polyethylene glycol 3350 within one day.

Data collection

X-ray diffraction data were collected at beamline 11C at Pohang Light Source II (PLS-II, Pohang, South Korea) with a Pilatus 6M detector (Dectris, Swiss). The FoADH crystals were equilibrated in a cryoprotectant buffer containing reservoir buffer plus 20% (v/v) ethylene glycol. ZoADH crystals were equilibrated in a cryoprotectant buffer containing reservoir buffer plus 20% (v/v) glycerol. The crystal was mounted on the goniometer and cooled under a nitrogen gas stream at 100 K. The diffraction data were indexed, integrated, and scaled using HKL2000 program (Otwinowski and Minor 1997). A data collection statistic is given in Table S2.

Structure determination

The electron density maps of FoADH and ZoADH were obtained via the molecular replacement method using the MOLREP program (Vagin and Teplyakov 2010). The crystal structure of an ADH from *Artemisia annua* (PDB code: 6LJH, unpublished) was used as search model for both FoADH and ZoADH. Model building and refinement were performed with the COOT program (Emsley and Cowtan 2004) and phenix.refinement in PHENIX (Liebschner et al. 2019), respectively. The geometry of final models was evaluated with MolProbity (Williams et al. 2018). Structural figures were generated with PyMOL (www.pymol.org). Structure-based sequence alignments were generated using Clustal-Omega (Sievers et al. 2011) and ESPript (Gouet et al. 1999). Tetrameric interfaces of ADHs were analyzed by PDBePISA (Krissinel and Henrick 2007). The interaction between ADHs and ligands were analyzed using PLIP (Salentin et al. 2015). The structure factor and coordinates are deposited in the Protein Data Bank under PDB codes 8H2A (FoADH-NAD) and 8H2B (ZoADH-NAD).

Enzyme activity determination and substrate screening

For determining the enzyme activity of the ADHs, the absorbance maximum of NADH at 340 nm was utilized. The absorbance at 340 nm was measured every minute over a 10 min

period using a microplate spectrophotometer (BioTek Synergy H1, Agilent Technologies, Santa Clara, CA, USA), and the slope over time was used to determine activities or relative activities. One unit of activity is defined as oxidation or formation of 1 µmol of NADH per minute. For calculation of activity, the molar absorption coefficient of NADH was determined via a standard curve that covered the range of 0 to 0.5 mM. For the initial substrate screening, several alcohols/aldehydes/ketones were employed at a final concentration of 10 mM. For increased substrate solubility, these reactions contained 3.5% (v/v) dimethyl sulfoxide (DMSO). The total volume for all reactions was 0.2 mL. The oxidation and reduction were both conducted at an incubation temperature of 70 °C. Reduction of aldehydes was performed in the presence of a 50 mM succinate buffer pH 6.5, while oxidation reactions were assayed in the presence of a 50 mM NaPi buffer pH 8.5. The final enzyme concentrations used to provide a linear absorbance increase or decrease ranged from 20-100 µg mL^{-1} for the oxidation reactions and from 0.25-2.5 µg mL^{-1} for the reduction reactions. The reaction was initialized by the addition of 0.5 mM NAD^+ or NADH. For the measurement with sugar substrates, a reduced reaction temperature of 40 °C and an increased measuring time of 30 min was chosen. Various sugars were used at a final substrate concentration of 30 mM. A concentration of 0.2% (w/v) was used for porphyran. Oxidation and reduction reactions were performed in the identical buffers as used for substrate screening, the final enzyme concentration was 0.1 mg mL^{-1}. The reaction was initialized by the addition of 0.5 mM NAD^+ or NADH. For the determination of cofactor utilization, the oxidation of 10 mM benzyl alcohol was performed in the presence of different NAD^+ or $NADP^+$ concentrations ranging from 0 to 5 mM in 50 mM HEPES buffer pH 8.5 at 25 °C and a final enzyme concentration of 0.1 mg mL^{-1}. For the determination of the kinetic parameters, a final protein content of 0.1 mg mL^{-1} (corresponding to a protein concentration of 2.44 µM) was used for the oxidation reactions. When determining K_m and V_{max} values for NAD^+, 15 mM benzyl alcohol was used as the final substrate concentration, while a final cofactor concentration of 5 mM NAD^+ was used for the measurement for benzyl alcohol. The oxidation reactions were carried out in 50 mM NaPi buffer pH 8.5 and at a reaction temperature of 70 °C. A final protein content of 5 µg mL^{-1} was used in the reduction reaction (corresponding to a protein concentration of 0.012 µM). For the determination of the kinetic parameters for NADH, 2.5 mM pyridine-3-carbaldehyde was used as the final substrate concentration, while a final cofactor concentration of 0.5 mM NADH was used for the determination of the kinetic parameters for pyridine-3-carbaldehyde. The reduction reactions were carried out in 50 mM succinate buffer pH 6.5 and at 70 °C. In order to test for thiol-dependent formaldehyde detoxification, different thiols were evaluated as potential cofactors. For this reaction, the thiol cofactor and formaldehyde were used in a 1:1 ratio at a final concentration of 0.5 mM. The measurement was performed in the 50 mM NaPi buffer pH 8.5 at 70 °C with a final enzyme concentration of 0.2 mg mL^{-1}. The reaction was started by the

addition of 0.5 mM NAD^+. The ADH catalyzed disproportionation of formaldehyde into methanol and formate was monitored by a pH change utilizing the phenol red assay (Martínez-Martínez et al. 2018). This measurement was performed in a microtiter plate and the reaction volume was 0.2 mL. 5 mM formaldehyde was used as substrate, 0.5 mM NAD^+ as cosubstrate and 0.1 mg mL^{-1} as final enzyme concentration. The pH indicator phenol red was used at a final concentration of 91 µM. The reaction was performed in a 5 mM HEPES buffer pH 8.5 at 40 °C. Absorbance at 560 nm was measured every minute for 20 min.

Influence of pH and buffer components

To determine the pH optimum of the enzymes, the oxidation and reduction reactions were both investigated in the presence of varying pH values. All buffers had a concentration of 50 mM. A citrate buffer was used in the pH range of 5 to 6, a NaPi buffer in the range of 6 to 8.5, a CHES buffer in the range of 8.5 to 10 and a CAPS buffer in the range of 10 to 12.5. The assay conditions for the oxidation reaction were as follows: the reaction volume was 200 µL, 10 mM benzyl alcohol and 0.5 mM NAD^+ was used as substrate. The reaction was started by the addition of 0.1 mg mL^{-1} ADH. For the reduction reaction, instead of benzyl alcohol and NAD^+, 10 mM benzaldehyde and 0.5 mM NADH were used. Since benzaldehyde was less soluble in the buffer than benzyl alcohol, both reactions contained 3.5% (v/v) DMSO, in order to achieve better comparability. The reaction was carried out at 25 °C in the respective buffers. To examine the influence of buffer components on enzyme activity, different buffers with a concentration of 50 mM were used. The buffers had a pH of 6.5 for the reduction reaction, whereas it was 8.5 for the oxidation reaction. The reaction was carried out under the same conditions as those for the pH optimum. Relative activities were determined as described above.

Influence of temperature and thermostability

The temperature optimum was determined by conducting the oxidation reaction at different temperatures in the range between 20 and 90 °C. For this, the reaction mixture without enzyme was preheated to the desired temperature in a reaction tube by using a heating block (Eppendorf ThermoMixer®C, Eppendorf SE, Hamburg, Germany) for at least 45 min. The reaction mixture had a volume of 200 µL. 30 mM benzyl alcohol and 0.5 mM NAD^+ were employed as substrates, and the reaction was carried out at different temperatures ranging from 20 to 90 °C in a 50 mM NaPi buffer pH 7.5. The reaction was initiated by the addition of enzyme with a final concentration of 0.1 mg mL^{-1}. For the thermostability determination, the purified ADH (1 mg mL^{-1}) was incubated in 50 mM NaPi buffer pH 7.5 for 1 or 4 h in a gradient thermal cycler (FlexCycler², Analytik Jena, Jena, Germany) at various temperatures ranging from 20 to 80 °C. Residual activity was then determined as described above and compared

with a control that was incubated on ice. The assay conditions were as follows: the reaction volume was 200 µL, the final enzyme concentration was 0.1 mg mL^{-1}, 10 mM benzyl alcohol was used as substrate, the reaction was performed at 40 °C in 50 mM NaPi buffer pH 7.5. The reaction was initiated by the addition of 0.5 mM NAD^+.

Influence of sodium chloride

Determination of NaCl influence on enzyme activity was performed by carrying out the oxidation reaction in the presence of different NaCl concentrations varying from 0 to 800 mM. The relative activities were determined as described above and were compared with a control where no additional NaCl was present. Assay conditions were as follows: the reaction volume was 200 µL, 10 mM benzyl alcohol was used as substrate, the final enzyme concentration was 0.1 mg mL^{-1} and the NaCl concentration was between 0 and 800 mM. The reaction was carried out at 25 °C in a 50 mM NaPi buffer pH 8.5 or in a 50 mM Tricine buffer pH 8.5 and started by the addition of 0.5 mM NAD^+.

Influence of metal ions and other small molecules

For the determination of the influence of various metal ions on enzyme activity, the ADHs with a concentration of 1 mg mL^{-1} were incubated with either 1 or 10 mM metal ion at RT for 1 h before activity measurement. A sample without additional metal ion served as a control. For the activity measurement, the standard assay was used with the following conditions: the reaction mixture had a total volume of 200 µL, 10 mM benzyl alcohol was used as substrate, a final enzyme concentration of 0.1 mg mL^{-1} was employed and the reaction was performed in 50 mM HEPES buffer pH 8.5 at 25 °C. The reaction was initiated by the addition of 0.5 mM NAD^+. In order to determine the effect of EDTA, dithiothreitol (DTT) and 2-mercaptoethanol (2-ME) on enzyme activity, the ADHs were incubated at a protein concentration of 1 mg mL^{-1} with these components at concentrations of 1, 10 or 25 mM for 1h at RT before activity determination. Higher concentrations up to 100 mM were additionally tested for EDTA. The untreated enzyme served as a control. The activity measurement was performed as described for the influence of metal ions.

Influence of solvents and formaldehyde

To evaluate the influence of selected water-miscible solvents on the activity of both ADHs, the oxidation reaction was conducted in the presence of 5, 10, and 20% (v/v) solvent and compared with a control containing no additional solvent. The relative activity was determined as described above. The total reaction volume was 0.2 mL and 0.1 mg mL^{-1} of enzyme was used as final enzyme concentration. The reactions were performed in 50 mM NaPi buffer at 25 °C. 10 mM benzyl alcohol was employed as substrate and the reactions were started by

adding 0.5 mM NAD^+. The enzymes were incubated at a concentration of 1 mg mL^{-1} with different concentrations of formaldehyde varying from 0 to 50 mM for 1 h at RT prior to activity measurement to evaluate the effect of formaldehyde on enzyme activity. Relative activity was determined as described above. For the activity measurement, the same conditions were used as for the influence of solvent.

Results

Distribution and gene neighborhood analysis

In order to obtain an overview regarding the distribution and function of these ADHs in marine bacteria, we queried the MarDB and MarRef databases for ADHs with similar sequences to FoADH and ZoADH and constructed a sequence similarity network based on an alignment score of 150 and a sequence identity of 63.14%. This analysis revealed six main clusters, which we define here as clusters containing at least 34 sequences, with FoADH and ZoADH included in main cluster 2 (Fig. S1). This main cluster primarily contained sequences that were annotated as zinc-dependent ADHs, histidine kinases, ADH GroES-like domains and some glutathione dependent formaldehyde dehydrogenases/ADHs. However, glutathione-dependent and mycothiol-dependent formaldehyde dehydrogenases were identified predominantly in clusters 1 and 4, respectively. Based on main cluster 2, we performed a genome neighborhood analysis to obtain a general sense of which genes are located in close proximity to the ADH gene. Similar genomic arrangements consisting of CYP, redox partners, an esterase and the ADH can be identified in several marine bacteria that are capable of degrading marine polysaccharides (Fig. S2), including members of the genera *Polaribacter*, *Maribacter* and *Arenibacter*. Minor differences in gene arrangement can be observed among some organisms such as *F. agariphila* or *Algibacter lectus*, where genes encoding for CAZymes (GH2 and GH16) are located between the ADH and the esterase gene. Additionally, some genes encoding for sulfatases and SusC/SusD homologs, which are responsible for the binding and transport of sugar molecules (Martens et al. 2009), are located up- and downstream of the ADH gene. Considering that the ADH gene consistently appears in the proximity of the genes, which encode for CAZymes and key enzymes for the oxidative demethylation of G6Me, it is conceivable that the ADH possesses a specific function in carbohydrate utilization or a subsequent reaction.

Knockout of the ADH encoding gene in *Z. galactanivorans* and growth studies

As an attempt to elucidate the biological relevance of the ADHs for the organisms, a knock-out of the gene, which encodes for the ADH in *Z. galactanivorans* was performed followed by growth experiments. The controls employed for these growth studies were the wild type (WT) and an additional knock-out strain of *Z. galactanivorans* in which the CYP gene was deleted.

When G6Me was employed as the sole carbon source, impaired growth was observed for the ADH and CYP knock-out strains, while the WT exhibited normal growth (Fig. 2). In contrast, regular growth was observable for all three strains in a control, which contained D-galactose as sole carbon source. Consequently, the ADH possessed an impact on the G6Me utilization of *Z. galactanivorans*.

Functional overexpression and purification of the ADHs

Since we could demonstrate a biological significance of the ADH for the utilization of G6Me by the gene knockout in *Z. galactanivorans*, our next aim was to identify the enzyme function. We therefore cloned the gene encoding for the ADH from *F. agariphila* into a pET28a vector. For the ADH from *Z. galactanivorans* a synthetic gene was ordered in the pET28a vector. Both enzymes were successfully overexpressed and purified (Fig. S3), which established the basis to elucidate putative biological functions of these ADHs by performing biochemical and structural biological characterizations.

Substrate spectrum of the ADHs

In order to obtain a preliminary understanding of the substrate spectrum of these ADHs, their ability for the alcohol oxidation as well as the reduction of various aldehydes and ketones were examined. Both enzymes converted predominantly aromatic substrates (Tables 1 and 2). The highest specific activity of 64.1 U mg^{-1} for FoADH and 54.9 U mg^{-1} for ZoADH was observed for the reduction of pyridine-3-carbaldehyde. In addition to compounds containing a benzene ring, substrates harboring a furan or thiophene ring, such as furfural and thiophene-3-carbaldhyde, were also preferentially converted. Positions of additional substituents at the benzene ring influenced the activity. A difference in the specific activities for the constitutional isomers of terephthalaldehyde and tolualdehyde were observed for both enzymes. In particular, substrates that possessed an additional substituent in *ortho*-position were converted significantly less efficiently. In addition, the length of the aldehyde substituent at the benzene ring also affected the activity. For instance, hydrocinnamaldehyde was converted by both enzymes, whereas for phenylacetaldehyde no activity was observable. In contrast to benzaldehyde, the structurally similar acetophenone could not be oxidized. Thus, both ADHs were unable to convert ketones to secondary alcohols. In comparison to the reduction reaction, significant reduced specific activities were noticed for the oxidation reactions (Table 2). Simultaneously, lower K_m values in the range of 0.6 to 0.8 mM could be determined for pyridine-3-carbaldehyde compared to the K_m values of 3.6 and 5.3 mM for benzyl alcohol (Fig. S4). The highest specific activity of 490 mU mg^{-1} for FoADH and 290 mU mg^{-1} for ZoADH was observed for 2,5-bis(hydroxymethyl)furan. Both ADHs lacked any activity for smaller aliphatic alcohols such as methanol and ethanol. Since the ADHs exhibited predominantly activities for

substrates containing a ring structure, several sugars were also considered as possible substrates. However, no activity was observed for the oxidation or reduction of galactose, G6Me and additional monosaccharides and disaccharides (Table S3). Additionally, the marine carbohydrate porphyran was also evaluated as a potential substrate, however, no activity was detected either. As mentioned earlier in the introduction, ADHs require either NAD^+ or $NADP^+$ as cofactor for their enzymatic activity. In order to identify the preferred cofactor for both ADHs, the oxidation of benzyl alcohol was conducted in the presence of varying NAD^+ and $NADP^+$ concentrations. Both ADHs utilize NAD^+ as cofactor, whereas in the presence of up to 5 mM $NADP^+$ no activity for the oxidation reaction was observed.

Testing for formaldehyde detoxification activity

Since activity was neither observed for galactose nor for G6Me, we hypothesized that the ADHs may participate in formaldehyde detoxification, considering that formaldehyde is formed as a by-product in the oxidative demethylation reaction. Members of the zinc-dependent ADHs may catalyze the glutathione-dependent formaldehyde detoxification, therefore various thiols were considered as potential cofactors. Thiol-dependent detoxification of formaldehyde proceeds via a spontaneous reaction between the sulfhydryl group of the thiol cofactor and the carbon atom of formaldehyde, resulting in the formation of an alcohol (Fig. 3a) (Chen et al. 2016). Subsequently, this alcohol can be oxidized by the ADH to a thioester, which is then converted by an esterase to formate and the starting thiol cofactor (Gonzalez et al. 2006). Based on the results of our genome neighborhood analysis, where we have also demonstrated that a gene encoding for an esterase is located in the vicinity of the ADH gene, it is quite possible that a thiol-dependent detoxification of formaldehyde can proceed via both enzymes. In addition to glutathione, mainly mycothiol (Misset-Smits et al. 1997; Newton and Fahey 2002) and bacillithiol (Newton et al. 2009; Chandrangsu et al. 2018) are well known cofactors in formaldehyde detoxification (Fig. 3b). However, no activity was detected for these thiols. Furthermore, common thiols abundant in nature such as cysteine, coenzyme A and L-ergothioneine (Hand and Honek 2005) were also investigated as cofactors. Nevertheless, no activity was observed for these substrates in combination with formaldehyde either. Considering that the ADHs mainly exhibited activity for aromatic substrates, aromatic thiols such as 2-mercaptoimidazole or 4-mercaptophenol were considered as possible substrates as well. However, even with these compounds, no oxidation reaction was detected. Furthermore, neither enzyme exhibited activity for the oxidation or reduction of formaldehyde in the presence of only NAD^+ or NADH as cofactors. In addition, a disproportionation reaction of formaldehyde into methanol and formate catalyzed by the ADH was also checked. However, no activity could be detected. Consequently, the ADHs possessed no activities for the substrate nor for the

products of the oxidative demethylation of G6Me. To provide additional insights into these ADHs, we performed further biochemical characterizations of both enzymes.

Influence of pH and buffer components on enzyme activity

In order to determine the optimal pH for the enzymatic reaction, several buffers were investigated in the pH range from 5.5 to 12.5. A similar pH optimum was observed for both enzymes (Fig. 4). The reduction reaction was most efficiently catalyzed at pH 6.5, while oxidation was found to be most efficient at pH 8.5 (Fig.4 a-b and d-e). At pH 5 and at 12.5, no activity was detected for either enzymes; precipitation was noticed at pH 5 while employing higher protein concentrations. Since a considerable difference in activity was observed between NaPi and CHES buffer at pH 8.5, other buffers were also evaluated at pH 6.5 (Fig. 4 c) and 8.5 (Fig. 4f) to investigate the influence of buffer components on the activity. For the oxidation reaction at pH 8.5, it was shown that by employing a Tris-HCl buffer, an approximately 60 to 80% increased activity was obtained compared to the activity in the NaPi buffer. In contrast, a significant activity decrease of 95% was observed for both enzymes in the presence of a borate-NaOH buffer. For the reduction reaction at pH 6.5, a slight increase in activity of ~8 to 16% could be detected using citrate and succinate buffer compared to the NaPi buffer, with the highest activity found for the succinate buffer.

Influence of temperature and enzyme thermostability

In addition to the pH value, the temperature influence is essential for enzymatic activity. At the same time, elevated temperatures promote substrate solubility and thus the application of higher concentrations which also may shift the reaction equilibrium towards product formation (Unsworth et al. 2007). Therefore, the impact of temperature in the range between 20 and 90 °C was investigated for both enzymes. The ADHs possessed a similar temperature profile, where activity increased with rising temperature, reaching an optimum between 65 to 75 °C (Fig. 5a). However, at higher temperatures the activity decreased rapidly, whereas at room temperature only a relative activity of about 18% for FoADH and 10% for ZoADH was observed. The measurement for the temperature optimum was performed for 10 min to ensure that any influence of thermostability would not affect the results. Thermostability of enzymes is an important parameter for biocatalysis, since many industrial processes operate at higher temperatures for longer time periods, leading to increased product yields. The thermostability of the ADHs was therefore evaluated next by incubating the enzymes for 1 or 4 h at various temperatures ranging from 20 to 80 °C followed by determination of residual activity. After 1 h incubation at 59 °C as well as lower temperatures, no decrease in activity was detected for FoADH compared to a control incubated on ice (Fig. 5b). Residual activity only diminished at

higher incubation temperatures and a residual activity of roughly 20% was still observed for 80 °C. In contrast, after 4 h incubation, almost no residual activity was observed at this temperature. Nevertheless, even after this extended incubation period, a high remaining activity of approximately ≤ 85% was detected for the temperature range of 20 to 59 °C. ZoADH exhibited a similar behavior in thermostability as FoADH, however an initial activity decrease of 20% was observed for the 1 h incubation already at 57 °C (Fig. 5c). A severe activity loss of almost 95 to 100% was observed for ZoADH when incubated for 4 h at temperatures >73 °C.

Influence of sodium chloride

Enzymes originating from marine organisms may possess habitat-related characteristics such as an increased salt tolerance (Trincone 2011). Considering that both enzymes originate from marine bacteria, the influence of NaCl on the enzyme activity was tested. For this purpose, the relative activities for the oxidation reaction were determined in the presence of different NaCl concentrations ranging from 0 to 800 mM in the NaPi and Tricine buffer, respectively. Both ADHs displayed a similar behavior in the presence of rising NaCl concentrations (Fig. S5). An increase in relative activity of approximately 10% was observed in the range from 0 to 150 mM NaCl for FoADH using the Tricine buffer. In contrast, only a minor increase in activity was observed for the NaCl concentration of 100 mM in the NaPi buffer. A difference between the NaCl influence depending on the selected buffer was also noticed for ZoADH, with a higher effect in the Tricine buffer. For ZoADH, an increase in relative activity of 20% was also detected in the range of 0 to 200 mM NaCl. At NaCl concentrations ≥ 400 mM, a diminished relative activity was observed for both enzymes.

Influence of metal ions and other small molecules

Both enzymes are annotated as zinc-dependent ADHs, which contain a catalytic zinc ion in the active site. An influence of various metal ions on the enzyme activity is thus possible and was therefore investigated next. For this purpose, the enzymes were incubated with different metal ions at concentrations of 1 or 10 mM for 1 h prior to activity measurement and the relative activities were determined. A high dependence on metal ions was observed for both ADHs, with nearly all ions assayed exhibiting a beneficial effect on enzyme activity (Table 3 and Fig. S6). Particularly higher concentrations of Ni^{2+}, Co^{2+} and Mn^{2+} led to a 10 to 14-fold increase in relative activity for both enzymes compared to the control which contained no additional metal ion. In contrast, complete inhibition for both enzymes was only observed for Cu^{2+}, Zn^{2+} as well as 10 mM Fe^{3+}. Additionally, we analyzed whether the chelating agent EDTA, which is capable of complexing bivalent metal ions, affects the enzymatic activity. After 1 h incubation in the presence of 25 mM EDTA, a reduction in the relative activity for both enzymes was found, while an almost complete inhibition was observable at an EDTA concentration of 100 mM

(Table 3 and Fig. S7). The influence of DTT and 2-mercaptoethanol (2-ME) on activity was also investigated, since these compounds can affect enzyme stability. DTT had a lesser impact on both enzymes than 2-ME. A major decline in relative activity of over 70% was observed for both enzymes after 1 h incubation with 10 mM 2-ME (Table 3 and Fig. S7). When compared to ZoADH, the effect of the reducing agents was more pronounced for the activity of FoADH.

Influence of solvents and formaldehyde

The influence of water-miscible solvents on the enzyme activity of both ADHs was also investigated. Increasing the amount of solvent in the reaction led to a decrease in the relative activity for all tested solvents (Fig. S8). Compared to the other solvents, methanol and DMSO had the weakest negative effects on the enzyme activity, leading to a relative activity of still 50% in the presence of 10% (v/v) solvent. In addition, the presence of formaldehyde on the enzyme activity was examined, since formaldehyde is released during the oxidative demethylation of G6Me and the ADHs are most likely involved in this reaction. Therefore, the ADHs were incubated with a variety of formaldehyde concentrations in the range between 0 and 50 mM for 1 h at RT and the relative activities was determined. In the presence of 0 to 1 mM formaldehyde, no reduction in activity was observed. An initial decrease in relative activity of approximately 10-20% could be perceived in the presence of 2.5 mM formaldehyde (Fig. S9). At higher formaldehyde concentrations, a more severe activity decrease was found, while no activity was observed for both enzymes in the presence of 50 mM formaldehyde.

Overall structures of FoADH and ZoADH

In order to gain a deeper understanding of the molecular function, we performed X-ray crystallography studies of FoADH and ZoADH. For the determination of the functional states of both ADHs, the essential NAD^+ cofactor was added to purified FoADH and ZoADH proteins before crystallization. The crystal structures of FoADH and ZoADH in complex with NAD^+ were determined at a resolution of 2.5 and 2.1 Å, respectively (Table S2). FoADH and ZoADH crystals belong to space group monoclinic $P2_1$ and orthorhombic $P2_12_12_1$, respectively and contain four and eight molecules in asymmetric unit, respectively (Fig. S10). The electron density map of FoADH and ZoADH clearly showed the almost entire polypeptide chain, except for a partially disordered fragment of the loop between the β5 and β6-strands (Gly111-His115 in both enzymes), which is involved in substrate binding and specificity. The monomer structures of FoADH and ZoADH comprise the catalytic domain (residues 1–149 and residues 283–326 for both enzymes) and the cofactor-binding domain (residues 150–282 for both enzymes) (Fig. 6a), which are separated by a cleft containing a deep pocket, which accommodates the substrate and the NAD^+ cofactor. The catalytic domain contains two zinc-binding sites, Zn1 and Zn2, which are responsible for catalytic activity and structural stability,

582 respectively. The cofactor binding domain adopts a typical Rossmann fold with the conserved
583 sequence “GXGXXG”. FoADH and ZoADH had a 76.0% similarity in amino acid sequence
584 (Fig. S11), and their monomer structures showed a similarity with a root-mean-square
585 deviation (r.m.s.d.) of 0.350-0.772 Å (Table S4).

586 In FoADH, molecules A/B/C/D and E/F/G/H form a tetrameric formation (Fig. S10). In
587 superimposition of monomeric FoADH molecules, the A, B, C, E and G molecules showed
588 structural similarity (denoted as closed form) with r.m.s.d. of 0.256-0.353 Å, whereas
589 molecules D and H (denoted as open form) showed the relatively high r.m.s.d. value of 0.457-
590 0.626 Å when superimposed with molecule A, B, C, E and G (Fig. 6b and Table S5). On the
591 other hand, molecule F maintains the intermediate conformation between the closed and open
592 conformations. When the cofactor binding domains of molecules A and H of FoADH were
593 superimposed, the catalytic binding of molecule H was shifted by approximately 2.0-3.3 Å in
594 the opposite direction of the substrate-binding cleft compared to molecule A (Fig. 6b).

595 In ZoADH, superimposition of molecules A, B and C exhibited a similar conformation (denoted
596 as closed form) with r.m.s.d of 0.198-0.226 Å, whereas molecule D (denoted as open form)
597 showed a relatively high r.m.s.d. value of 0.314-0.471 Å when superimposed with molecules
598 A, B and C (Fig. 6b and Table S6). Superposition of the cofactor binding domains of molecules
599 A and D clearly revealed the conformational difference between the catalytic domains. The
600 catalytic domain of molecule D is shifted about 2.2-3.3 Å to the outside of the substrate binding
601 cleft of ZoADH compared to molecule A. Accordingly, in the structure of NAD^+-bound FoADH,
602 molecules A/B/C and D represent closed and open conformations of the substrate binding site,
603 respectively. Collectively, the crystal structures of NAD^+-bound ZoADH and FoADH contain
604 the open and closed conformations between catalytic and cofactor-binding domains (see
605 below).

606 The crystal structures of FoADH and ZoADH showed the tetrameric formation via the
607 arrangement of a dimer of dimers (Fig. 6c). In both ADHs, the β17 and β18-strands of the
608 cofactor binding domains are stabilized by forming an antiparallel β-sheet with the β17* and
609 β18*strands (asterisk indicates the second monomer), respectively (Figs. S12 and S13). For
610 FoADH, the dimeric interface is stabilized by the main chain interactions of Ile297-Ile299*
611 (* denoting the partner molecule) and Ile299-Ile297* between the β17 strands and Tyr310-
612 Tyr310* between β18 strands (Fig. S12). In addition, numerous hydrogen and salt bridges
613 were observed in the dimer interface with a buried surface area of 1654 $Å^2$ (Table S7). The
614 dimer of dimers was stabilized by hydrogen interaction and the buried interface of dimers of
615 dimers is 1193 $Å^2$ (Table S7). For ZoADH, the dimeric interface is stabilized by the main chain
616 interactions of Ile298-Ile300* and Ile300-Ile298* between the β17 strand and Tyr311-Tyr311*
617 between β18 strand (Fig. S13). Moreover, numerous hydrogen and salt bridges were observed

at the dimer interface with a buried surface area of 1640 Å^2 (Table S8). The dimer of dimers was stabilized by hydrogen interactions and salt bridges and the buried interface of dimers of dimers is ~1205 Å^2 (Table S8). All active sites of the tetrameric ADH in the crystal were exposed to solvent (Fig. 6c). Superposition of tetrameric molecules of FoADH and ZoADH in the asymmetric unit shows an r.m.s.d. of 0.327-0.888 Å for whole Cα atoms (Fig. 6d).

Structural homology search by DALI revealed that both FoADH and ZoADH share structural similarities to the class II alcohol dehydrogenase (ADH4) from human (PDB code: 3COS, Z-score= 45.8 for FoADH and 45.3 for ZoADH, sequence identity= 32% for FoADH [357α atoms] and 30% for ZoADH [357α atoms]), an ADH from *E. coli* (PDB code: 5vm2, Z-score= 48.1 for FoADH and 38.1 for ZoADH, sequence identity= 28% for FoADH [329α atoms] and 27% for ZoADH [328α atoms]) as well as an ADH from *Thermotoga maritima* (PDB code: 3IP1, Z-score= 35.8 for FoADH and 36.8 for ZoADH, sequence identity= 25% for FoADH [328α atoms] and 23% for ZoADH [332α atoms]). Although these structural homologous ADHs share low amino acid sequence similarities with less than 32% compared to FoADH and ZoADH, the active site residues involved in the Zn^{2+} and NAD^+ binding are highly conserved (Fig. S11). In addition, the NAD^+-binding domain exhibits a typical Rossmann fold motif and has the classical conserved sequence “GXGXXG” as in other ADHs and the topologies of those ADHs are highly similar (Fig. S11). The overall topology of those homolog structures was similar with FoADH and ZoADH (Fig. S14). However, superimposition of those ADH structures revealed that there is a large difference in conformation between catalytic and cofactor-binding domains with a r.m.s.d. of 1.373-2.963 Å for FoADH and 1.376-2.191 for ZoADH (Fig. 6e), indicating that they possess large distinct NAD^+ and substrate-binding clefts. Meanwhile, ADHs from *E. coli* and *T. maritima* also formed the tetrameric formation in crystal structures like FoADH and ZoADH (Fig. S14). These ADHs have the similar tetrameric assembly, however the superimposition of the tetrameric ADHs showed that these tetrameric assemble have low similarity with a r.m.s.d of 17.68~29.94 Å.

NAD^+ and Zn^{2+}-binding sites of FoADH and ZoADH

While NAD^+ is the required cofactor for alcohol oxidation, Zn^{2+} interacts with the alcohol molecule in the active site. The electron density maps of a NAD^+ molecule and two zinc ions are clearly observed in a substrate binding cleft of both FoADH and ZoADH (Fig. S15). The binding configuration of NAD^+ and the Zn^{2+} ions of ZoADH and FoADH are highly similar (Fig. 7a). The adenine ring of NAD^+ was located in the hydrophobic pocket formed by hydrophobic interaction (Ile219, Leu245, Thr268, Ile270 and Leu273 for FoADH, Ile220, Leu246, Thr269, Ile271 and Leu274 for ZoADH). The adenine ribose appears to be in a C2’-endo conformation, and the O2’ and O3’ -hydroxyl group of ribose forms a hydrogen bond with the side chain of aspartate (Asp218 for FoADH and Asp219 for ZoADH). The pyrophosphate

moiety of the NAD^+ interacts with the nitrogen atoms of the main chain of glycine-valine residue (Gly197-Val198 for FoADH and Gly198 and Val199 for ZoADH) that forms the loop between strand β5 and helix α4. The nicotinamide ribose is in a C2'-endo conformation, and hydrogen bonds are formed between the ribose O2' -hydroxyl group and threonine (Thr43 for FoADH and ZoADH). The nicotinamide ring is in the anti-conformation. The carboxamide nitrogen atom of the nicotinamide ring interacted with main-chain of proline (Pro313 for FoADH and Pro314 for ZoADH) and valine (Val290 for FoADH and Val291 for ZoADH). The carboxamide oxygen atom of the nicotinamide ring interacted with main-chain of tyrosine (Tyr315 for FoADH and Tyr316 for ZoADH). Therefore, in both FoADH and ZoADH, the NAD^+ molecules are stabilized by hydrophobic and hydrogen bonds interactions.

In both FoADH and ZoADH, two zinc ions are commonly observed in the active site (Zn1 site) and in a loop between α2 and β7 (Zn2 site) (Fig. 7a and Fig. S15). The zinc ion at Zn1 site is coordinated by conserved cysteine and histidine residues (Cys41, His58, and Cys169 for FoADH and Cys41, His58, and Cys170 for FoADH) in the catalytic domain. The zinc ion at Zn2 site is involved in the protein stability and is tetrahedrally coordinated by conserved cysteine residues (Cys88, Cys91, Cys94, and Cys102 for both enzymes) (Fig. S15). There result indicated that ZoADH and FoADH showed high structural similarity for the NAD^+ and zinc binding configuration.

Different structural conformations were observed between monomeric ADHs in the tetrameric formation of FoADH and ZoADH (Fig. 6b), indicating that they exhibit structurally different substrate binding cleft and active site. In both results of superimposition of the active sites of FoADH and ZoADH, the positions of the NAD^+ and Zn2 sites were similar, whereas a significant difference was observed in the positions of the catalytic Zn1 sites (Fig. 7b). In FoADH and ZoADH, the maximum distances between metals from the Zn1 site were 2.57 and 2.60 Å, respectively, from closed and open conformation of two domains of ADHs (Fig. 7b).

Since the substrate binds to the Zn1 site and a dehydrogenase reaction occurs through the interaction of NAD^+ with the hydroxyl group, the size of the space between NAD^+ and Zn1 is involved in substrate selectivity. The closest/longest distance between the Zn^{2+} and C5 atom of the nicotinamide ring of NAD^+ in FoADH and ZoADH were 3.21/4.91 Å, and 3.46/5.49 Å, respectively (Fig. 7c). These different distance between Zn^{2+} and NAD^+ were caused by different from closed and open conformation of FoADH and ZoADH.

The electrostatic surfaces of FoADH and ZoADH showed that the substrate binding sites commonly exhibited a hydrophobic surface (Fig. 7c). The space of the substrate binding site of FoADH in closed and open conformation were approximately 3.4 x 4.2 Å and 3.9 x 5.4 Å, respectively (Fig. S15). In the closed and open conformation of FoADH, His42 and Ala270 are apart by 3.60 and 5.60 Å, respectively, showing the both surface structure surrounding the

690 NAD^+ (Fig. 7c). ZoADH also exhibits open and closed conformations similar to FoADH, but the
691 distance of open conformation is relatively wide. The space of the substrate binding site of
692 ZoADH in closed and open conformation were approximately 3.0 x 3.8 Å and 3.8 x 4.9 Å,
693 respectively (Fig. S15). In the closed conformation of ZoADH, the catalytic domain and the
694 cofactor domain are close to each other, especially His42 and Ala270 by a distance of 3.88 Å,
695 indicating the surface structure surrounding the NAD^+ (Fig. 7c). On the other hand, in the open
696 conformation of ZoADH, His42 and Ala270 are apart by 6.81 Å, and accordingly, the entire
697 NAD^+ molecule in the surface structure is exposed to the solvent (Fig. 7c).

698

699 ## Discussion

700 In the present work, FoADH from *F. agariphila* KMM 3901^T and ZoADH from *Z. galactanivorans*
701 $Dsij^T$ were characterized in detail to draw conclusions about their biological function. Three
702 main conclusions regarding the biological function can be derived by the knockout of the genes
703 encoding for ZoADH and CYP in *Z. galactanivorans* and subsequent growth studies on
704 D-galactose and G6Me. First, we confirmed the hypothesis of Reisky et al. that in the absence
705 of CYP-catalyzed oxidative demethylation, a G6Me utilization as sole carbon source is
706 infeasible for the organism (Reisky et al. 2018). Surprisingly, knockout of the ZoADH gene also
707 caused diminished growth of *Z. galactanivorans* in the presence of G6Me. Second, due this
708 observation, we can conclude a significant role of this ADHs in G6Me utilization in these marine
709 bacteria. From an ecological perspective, this has additional importance for the marine
710 carbohydrate degraders. G6Me can occur up to 28% within the porphyran chain (Rees and
711 Conway 1962). Thus, a reduced utilization of G6Me would represent a substantial potential
712 loss as a carbon source for the organism. Third, since normal growth was observed in the
713 presence of D-galactose as sole carbon source, a function in D-galactose metabolism can be
714 excluded. This was also supported by the observation that both ADHs lacked activity for
715 D-galactose. The ADHs are therefore probably involved in oxidative demethylation or a
716 subsequent reaction. Since no activity was observed for G6Me, the substrate of oxidative
717 demethylation could be excluded. Consequently, we hypothesized that the ADHs are involved
718 in the detoxification of formaldehyde, which is a by-product of the oxidative demethylation
719 reaction. This was also supported by the resistance of both ADHs to formaldehyde exposure.
720 Formaldehyde is a toxic metabolite due to its properties as a highly reactive electrophile. It can
721 react with free amino and thiol groups of proteins and nucleic acids, leading to protein and
722 DNA damages as well as cross-link formations (Chen et al. 2016; Shishodia et al. 2018; Tayri-
723 Wilk et al. 2020). It has been shown that higher concentrations of formaldehyde can negatively
724 affect the growth of *Z. galactanivorans* (Brott et al. 2022). Thus, a reduced growth of the ADH
725 knock-out strain could be explained by the potential accumulation of formaldehyde. There are

numerous metabolic pathways in which formaldehyde can be detoxified (Yurimoto et al. 2005; Klein et al. 2022). However, in the thiol-dependent formaldehyde detoxification, a zinc-dependent ADH and an esterase perform the key reactions (Sanghani et al. 2000; Gonzalez et al. 2006). Genome neighborhood analysis revealed that in most marine bacteria that possess the ADH gene, it was located in close proximity to a gene encoding for an esterase in addition to the CYP gene. We therefore investigated whether the ADH catalyzed a thiol-dependent detoxification of formaldehyde. However, with glutathione, mycothiol, and bacillithiol as thiol cofactors, no activity was detected for either ADH. These observations can be further explained with the crystal structures of both ADHs; sterically demanding compounds such as mycothiol or bacillithiol cannot fit into the narrow active site of these enzymes. These observations are also consistent with the results from the sequence similarity network, in which glutathione- and mycothiol-dependent formaldehyde dehydrogenases were predominantly present in different clusters (main clusters 1 and 4) than the ADHs (main cluster 2). Since no activity could be detected with literature-known cofactors, additional thiols were considered; however, no activity could be observed either. Thiol cofactors are still being discovered (Newton and Rawat 2019), perhaps marine organisms also possess an unidentified thiol, which can serve as a cofactor for this reaction. Since no activity was observed for formaldehyde without an additional thiol cofactor, the biological function of a thiol-independent formaldehyde dehydrogenase was excluded. In addition, some ADHs can possess dismutase activities (Trivić et al. 1999). A formaldehyde dismutase catalyzes the disproportionation of formaldehyde to methanol and formic acid in the presence of a covalent-bound NAD^+ (Yonemitsu and Kikuchi 2018). However, this reaction could not be detected. Both organisms harbor other metabolic pathways for the detoxification of formaldehyde (Brott et al. 2022). For instance, in *Z. galactanivorans*, the genes encoding for the key enzymes of the ribulose monophosphate pathway are upregulated in the presence of porphyran (Brott et al. 2022), so an accumulation of formaldehyde is unlikely. Eventually, the ADHs might have a completely different biological function such as the regeneration of NADH (Hilberath et al. 2021; Kokorin et al. 2021). In the oxidative demethylation reaction, NADH is oxidized to NAD^+, a reduced growth in the ADH knockout strain due to cofactor depletion might be possible. NADH could be regenerated by oxidation of an unknown component or by the thiol-dependent formaldehyde detoxification pathway. However, it is doubtful that the loss of one single enzyme would cause such a tremendous effect on NADH/NAD^+ homeostasis. Additionally, the ADHs displayed predominantly activity for the reduction of aldehydes under NADH consumption, therefore recycling of a cofactor is improbable.

Both ADHs possessed predominantly activity for aromatic substances, resulting in a substrate specificity resembling partially those of cinnamyl alcohol and/or benzyl alcohol dehydrogenases (Larroy et al. 2002; Willson et al. 2022). However, the highest activity was

observed for pyridine-3-carbaldehyde and furan derivatives. Furfural is generally produced as a side product by pretreating lignocellulosic biomass for the production of bioethanol. Under acidic conditions and high temperatures, dehydration of pentoses and hexoses proceeds, leading to the formation of furfural or hydroxymethylfurfural. Furfural acts as an inhibitor in subsequent bioethanol-producing fermentations by bacteria by prolonging the lag phase of growth and thereby the fermentation time (Mariscal et al. 2016). Consequently, these marine bacteria possess ADHs that catalyze the potential removal of furfural although the biological function may be different. The ADHs lacked activity for various sugar substrates, which excluded a polyol dehydrogenase activity. Activity for any other monosaccharides, disaccharides or even oligosaccharides formed during porphyran degradation is unlikely as well, considering the substrate specificity of the enzymes based on the narrow active site. The data from biochemical characterizations are discussed in the SI.

We have determined the crystal structures of FoADH and ZoADH complexed with NAD^+ and two zinc ions. These ADHs showed high structural similarity in terms of topology and assembly. On the one hand, these two ADHs showed similarities in topology with other ADHs from human, *E. coli* and *T. maritima*, but showed distinct conformation between the cofactor and catalytic domains of those ADHs. On the other hand, the crystal structures of FoADH and ZoADH showed open and closed conformations, indicating that the conformation between the two domains can change in the state where the substrate is not bound. These distinct conformations of FoADH and ZoADH represent different substrate binding pockets. When they exhibit an open conformation between the two domains of FoADH and ZoADH, they form a broadened substrate-binding pocket. Accordingly, in terms of substrate accessibility, we consider that substrate accessibility will be easier when FoADH and ZoADH have an open conformation.

During substrate recognition, when the converting functional group from the substrate approaches the Zn1 site on the substrate binding pocket of FoADH and ZoADH, the rest of the substrate is exposed to the nicotinamide of NAD^+ or the hydrophobic surface. Considering that the nicotinamide group of NAD^+ is involved in the oxidoreductase mechanism of the ADH, the substrate would prefer to be located to the hydrophobic surface rather than the nicotinamide group of NAD^+. Accordingly, FoADH and ZoADH may prefer substrates having a hydrophobic body. Our biochemical studies showed that both enzymes prefer aromatic substrates. We expected that the aromatic ring of the substrate may be located on a hydrophobic surface nearby the substrate binding pocket of FoADH and ZoADH. In this case, the aromatic ring of the substrate could interact with the Phe136 residue in the hydrophobic surfaces of the enzymes. Based on the active site structures of both ADH computational docking of a substrate will be able to provide an insight into the molecular mechanism and substrate specificity.

However, from the results of this study, ZoADH and FoADH have various conformations between catalytic and cofactor binding domain in NAD^+ and two zinc ion binding states, indicating the computational docking results could be different depending on the applied model structure. Also, based on our results, we concluded that the docking results may be different from biochemical experiments if the active sites of ZoADH and FoADH may have different conformations. Therefore, to better understand the substrate specificity, the crystal structures of ZoADH and FoADH in complex with the biological substrate will be needed in the future.

In summary, in this study we determined the putative functions of conserved ADH from marine *Flavobacteriia*. Additionally, we provided the crystal structures of the enzymes of *F. agariphila* and *Z. galactanivorans*. Enzymatic studies revealed the preferential conversion of aromatic aldehydes. We revealed that these enzymes are not involved in formaldehyde detoxification or in subsequent reaction of the oxidative demethylation of G6Me. Based on gene knockouts, we demonstrated the essential role of these ADHs in the utilization of marine algal sugars. Our study indicates a potential auxiliary activity of these ADHs in the utilization of marine sugars by marine *Flavobacteriia*.

Declarations

Funding: François Thomas acknowledges support from the French government via the National Research Agency program ALGAVOR (ANR-18-CE02-0001). We thank the German Research Foundation (DFG) for funding through the Research Unit FOR2406 "Proteogenomics of Marine Polysaccharide Utilization" (POMPU) (grants# BO 1862/17-1 and BO 1862/17-2 to U.T.B. and SCHW 595/10-2 to T.S.).

Conflicts of interests: The authors have no relevant financial or non-financial interests to disclose.

Author contributions: M.G., T.S. and U.T.B. initiated the study and directed the project. F.T. conducted the growth studies and created the knock-out strain. K.H.N performed the crystallization and structural analyses. T.D. performed the computational analysis. L. R. and H.C.G. performed the cloning and initial experiments on enzyme function of FoADH. S.B. and M.B. expressed and purified the enzymes and performed further experiments on enzyme function and characterization. S.B. and K.H.N prepared the main manuscript, which was revised by F.T., T.D, H.C.G., L. R., M.G, T.S. and U.T.B. and was approved by all authors.

Ethical approval: Not applicable.

Data availability: The datasets generated during and/or analyzed during the current study are available from the corresponding author on reasonable request.

References

Achkor H, Díaz M, Fernández MR, Biosca JA, Parés X, Martínez MC (2003) Enhanced formaldehyde detoxification by overexpression of glutathione-dependent formaldehyde dehydrogenase from *Arabidopsis*. Plant Physiol 132:2248-2255. https://doi.org/10.1104/pp.103.022277

Arnosti C, Wietz M, Brinkhoff T, Hehemann JH, Probandt D, Zeugner L, Amann R (2021) The biogeochemistry of marine polysaccharides: sources, inventories, and bacterial drivers of the carbohydrate cycle. Annu Rev Mar Sci 13:81–108. https://doi.org/10.1146/annurev-marine-032020-012810

Bauer M, Kube M, Teeling H, Richter M, Lombardot T, Allers E, Würdemann CA, Quast C, Kuhl H, Knaust F, Woebken D, Bischof K, Mussmann M, Choudhuri J V., Meyer F, Reinhardt R, Amann RI, Glöckner FO (2006) Whole genome analysis of the marine Bacteroidetes "*Gramella forsetii*" reveals adaptations to degradation of polymeric organic matter. Environ Microbiol 8:2201–2213. https://doi.org/10.1111/j.1462-2920.2006.01152.x

Bäumgen M, Dutschei T, Bartosik D, Suster C, Reisky L, Gerlach N, Stanetty C, Mihovilovic MD, Schweder T, Hehemann J-H, Bornscheuer UT (2021a) A new carbohydrate-active oligosaccharide dehydratase is involved in the degradation of ulvan. J Biol Chem 297:101210. https://doi.org/https://doi.org/10.1016/j.jbc.2021.101210

Bäumgen M, Dutschei T, Bornscheuer UT (2021b) Marine Polysaccharides: Occurrence, Enzymatic Degradation and Utilization. ChemBioChem 22:2247–2256. https://doi.org/10.1002/cbic.202100078

Brott S, Thomas F, Behrens M, Methling K, Bartosik D, Dutschei T, Lalk M, Michel G, Schweder T, Bornscheuer UT (2022) Connecting Algal Polysaccharide Degradation to Formaldehyde Detoxification. ChemBioChem 23:e202200269. https://doi.org/10.1002/cbic.202200269

Brunet M, de Bettignies F, Le Duff N, Tanguy G, Davoult D, Leblanc C, Gobet A, Thomas F (2021) Accumulation of detached kelp biomass in a subtidal temperate coastal ecosystem induces succession of epiphytic and sediment bacterial communities. Environ Microbiol 23:1638–1655. https://doi.org/10.1111/1462-2920.15389

Chandrangsu P, Loi V Van, Antelmann H, Helmann JD (2018) The role of bacillithiol in Gram-Positive *Firmicutes*. Antioxid Redox Signal 28:445–462. https://doi.org/10.1089/ars.2017.7057

Chen NH, Djoko KY, Veyrier FJ, McEwan AG (2016) Formaldehyde stress responses in bacterial pathogens. Front Microbiol 7:257. https://doi.org/10.3389/fmicb.2016.00257

de Lorenzo V, Timmis KN (1994) Analysis and construction of stable phenotypes in gram-negative bacteria with Tn5- and Tn10-derived minitransposons. Methods Enzymol 235:386–405. https://doi.org/10.1016/0076-6879(94)35157-0

Emsley P, Cowtan K (2004) Coot: model-building tools for molecular graphics. Acta Crystallogr D 60:2126–2132. https://doi.org/10.1107/S0907444904019158

Ficko-Blean E, Préchoux A, Thomas F, Rochat T, Larocque R, Zhu Y, Stam M, Génicot S, Jam M, Calteau A, Viart B, Ropartz D, Pérez-Pascual D, Correc G, Matard-Mann M, Stubbs KA, Rogniaux H, Jeudy A, Barbeyron T, Médigue C, Czjzek M, Vallenet D, McBride MJ, Duchaud E, Michel G (2017) Carrageenan catabolism is encoded by a complex regulon in marine heterotrophic bacteria. Nat Commun 8:1685. https://doi.org/10.1038/s41467-

879 017-01832-6

880 Field CB (1998) Primary production of the biosphere: Integrating terrestrial and oceanic
881 components. Science 281:237–240. https://doi.org/10.1042/bst0040954

882 Gonzalez CF, Proudfoot M, Brown G, Korniyenko Y, Mori H, Savchenko A V., Yakunin AF
883 (2006) Molecular basis of formaldehyde detoxification: Characterization of two
884 S-formylglutathione hydrolases from *Escherichia coli*, FrmB and YeiG. J Biol Chem
885 281:14514–14522. https://doi.org/10.1074/jbc.M600996200

886 Gouet P, Courcelle E, Stuart DI, Métoz F (1999) ESPript: analysis of multiple sequence
887 alignments in PostScript. Bioinformatics 15:305–308.
888 https://doi.org/10.1093/bioinformatics/15.4.305

889 Grondin JM, Tamura K, Déjean G, Abbott DW, Brumer H (2017) Polysaccharide utilization loci:
890 Fueling microbial communities. J Bacteriol 199:e00860-16.
891 https://doi.org/10.1128/JB.00860-16

892 Gutheil WG, Holmquist B, Vallee BL (1992) Purification, Characterization, and partial
893 sequence of the Glutathione-Dependent Formaldehyde Dehydrogenase from *Escherichia*
894 *coli*: A Class III Alcohol Dehydrogenase. Biochemistry 31:475–481.
895 https://doi.org/10.1021/bi00117a025

896 Hall M, Bommarius AS (2011) Enantioenriched compounds via enzyme-catalyzed redox
897 reactions. Chem Rev 111:4088–4110. https://doi.org/10.1021/cr200013n

898 Hambidge M, Cousins RJ, Costello RB (2000) Zinc and health: Current status and future
899 directions: Introduction. J Nutr 130:1344S-1349S.

900 Hand CE, Honek JF (2005) Biological chemistry of naturally occurring thiols of microbial and
901 marine origin. J Nat Prod 68:293–308. https://doi.org/10.1021/np049685x

902 Hilberath T, Raffaele A, Windeln LM, Urlacher VB (2021) Evaluation of P450 monooxygenase
903 activity in lyophilized recombinant *E. coli* cells compared to resting cells. AMB Express
904 11:162. https://doi.org/10.1186/s13568-021-01319-0

905 Klein VJ, Irla M, López MG, Brautaset T, Brito LF (2022) Unravelling formaldehyde metabolism
906 in bacteria: Road towards Synthetic Methylotrophy. Microorganisms 10:220.
907 https://doi.org/10.3390/microorganisms10020220

908 Klemetsen T, Raknes IA, Fu J, Agafonov A, Balasundaram V, Tartari G, Robertsen E,
909 Willassen NP (2018) The MAR databases : development and implementation of
910 databases specific for marine metagenomics. Nucleic Acids Res 46:692–699.
911 https://doi.org/10.1093/nar/gkx1036

912 Koesoema AA, Standley DM, Senda T, Matsuda T (2020) Impact and relevance of alcohol
913 dehydrogenase enantioselectivities on biotechnological applications. Appl Microbiol
914 Biotechnol 104:2897–2909. https://doi.org/10.1007/s00253-020-10440-2

915 Kokorin A, Parshin PD, Bakkes PJ, Pometun AA, Tishkov VI, Urlacher VB (2021) Genetic
916 fusion of P450 BM3 and formate dehydrogenase towards self-sufficient biocatalysts with
917 enhanced activity. Sci Rep 11:21706. https://doi.org/10.1038/s41598-021-00957-5

918 Kracher D, Ludwig R (2016) Cellobiose dehydrogenase: An essential enzyme for
919 lignocellulose degradation in nature - A review. Die Bodenkultur J L Manag Food Environ
920 67:145–163. https://doi.org/10.1515/boku-2016-0013

921 Krause-Jensen D, Duarte CM (2016) Substantial role of macroalgae in marine carbon
922 sequestration. Nat Geosci 9:737–742. https://doi.org/10.1038/ngeo2790

923 Krissinel E, Henrick K (2007) Inference of macromolecular assemblies from crystalline state.

924 J Mol Biol 372:774–797. https://doi.org/10.1016/j.jmb.2007.05.022

925 Lapébie P, Lombard V, Drula E, Terrapon N, Henrissat B (2019) Bacteroidetes use thousands
926 of enzyme combinations to break down glycans. Nat Commun 10: 2043.
927 https://doi.org/10.1038/s41467-019-10068-5

928 Larroy C, Parés X, Biosca JA (2002) Characterization of a *Saccharomyces cerevisiae*
929 NADP(H)-dependent alcohol dehydrogenase (ADHVII), a member of the cinnamyl alcohol
930 dehydrogenase family. Eur J Biochem 269:5738–5745. https://doi.org/10.1046/j.1432-
931 1033.2002.03296.x

932 Li C, Wen A, Shen B, Lu J, Huang Y, Chang Y (2011) FastCloning: a highly simplified,
933 purification-free, sequence- and ligation-independent PCR cloning method. BMC
934 Biotechnol 11:92. https://doi.org/10.1186/1472-6750-11-92

935 Liebschner D, Afonine P V, Baker ML, Bunkóczi G, Chen VB, Croll TI, Hintze B, Hung LW,
936 Jain S, McCoy AJ, Moriarty NW, Oeffner RD, Poon BK, Prisant MG, Read RJ, Richardson
937 JS, Richardson DC, Sammito MD, Sobolev O V, Stockwell DH, Terwilliger TC,
938 Urzhumtsev AG, Videau LL, Williams CJ, Adams PD (2019) Macromolecular structure
939 determination using X-rays, neutrons and electrons: recent developments in Phenix. Acta
940 Crystallogr D 75:861–877. https://doi.org/10.1107/S2059798319011471

941 Lu F, Xu W, Zhang W, Guang C, Mu W (2019) Polyol dehydrogenases: intermediate role in
942 the bioconversion of rare sugars and alcohols. Appl Microbiol Biotechnol 103:6473–6481.
943 https://doi.org/10.1007/s00253-019-09980-z

944 Mariscal R, Maireles-Torres P, Ojeda M, Sádaba I, López Granados M (2016) Furfural: A
945 renewable and versatile platform molecule for the synthesis of chemicals and fuels.
946 Energy Environ Sci 9:1144–1189. https://doi.org/10.1039/c5ee02666k

947 Martens EC, Koropatkin NM, Smith TJ, Gordon JI (2009) Complex glycan catabolism by the
948 human gut microbiota: The Bacteroidetes sus-like paradigm. J Biol Chem 284:24673–
949 24677. https://doi.org/10.1074/jbc.R109.022848

950 Martínez-Martínez M, Coscolín C, Santiago G, Chow J, Stogios PJ, Bargiela R, Gertler C,
951 Navarro-Fernández J, Bollinger A, Thies S, Méndez-García C, Popovic A, Brown G,
952 Chernikova TN, García-Moyano A, Bjerga GEK, Pérez-García P, Hai T, Del Pozo M V.,
953 Stokke R, Steen IH, Cui H, Xu X, Nocek BP, Alcaide M, Distaso M, Mesa V, Peláez AI,
954 Sánchez J, Buchholz PCF, Pleiss J, Fernández-Guerra A, Glöckner FO, Golyshina O V.,
955 Yakimov MM, Savchenko A, Jaeger KE, Yakunin AF, Streit WR, Golyshin PN, Guallar V,
956 Ferrer M (2018) Determinants and Prediction of Esterase Substrate Promiscuity Patterns.
957 ACS Chem Biol 13:225–234. https://doi.org/10.1021/acschembio.7b00996

958 Misset-Smits M, Van Ophem PW, Sakuda S, Duine JA (1997) Mycothiol, 1-*O*-(2'-[*N*-acetyl-L-
959 cysteinyl]amido-2'-deoxy-α-D-glucopyranosyl)-D-myo-inositol, is the factor of NAD/factor-
960 dependent formaldehyde dehydrogenase. FEBS Lett 409:221–222.
961 https://doi.org/10.1016/S0014-5793(97)00510-3

962 Newton GL, Fahey RC (2002) Mycothiol biochemistry. Arch Microbiol 178:388–394.
963 https://doi.org/10.1007/s00203-002-0469-4

964 Newton GL, Rawat M (2019) N-methyl-bacillithiol, a novel thiol from anaerobic bacteria. MBio
965 10:e02634-18. https://doi.org/10.1128/mBio.02634-18

966 Newton GL, Rawat M, La Clair JJ, Jothivasan VK, Budiarto T, Hamilton CJ, Claiborne A,
967 Helmann JD, Fahey RC (2009) Bacillithiol is an antioxidant thiol produced in Bacilli. Nat
968 Chem Biol 5:625–627. https://doi.org/10.1038/nchembio.189

969 Otwinowski Z, Minor W (1997) Processing of X-ray diffraction data collected in oscillation
970 mode. In: Carter CW (ed) Macromolecular Crystallography Part A. Methods Enzymol

276:307-326. https://doi.org/10.1016/S0076-6879(97)76066-X

Shannon P, Markiel A, Ozier O, Baliga NS, Wang JT, Ramage D, Amin N, Schwikowski B, Ideker T (2003) Cytoscape: a software environment for integrated models of biomolecular interaction networks. Genome Res 13:2498-2504. https://doi.org/10.1101/gr.1239303.metabolite

Persson B, Hedlund J, Jörnvall H (2008) Medium- and short-chain dehydrogenase/reductase gene and protein families: The MDR superfamily. Cell Mol Life Sci 65:3879–3894. https://doi.org/10.1007/s00018-008-8587-z

Pick A, Rühmann B, Schmid J, Sieber V (2013) Novel CAD-like enzymes from *Escherichia coli* K-12 as additional tools in chemical production. Appl Microbiol Biotechnol 97:5815–5824. https://doi.org/10.1007/s00253-012-4474-5

Priyam A, Woodcroft BJ, Rai V, Moghul I, Munagala A, Ter F, Chowdhary H, Pieniak I, Maynard LJ, Gibbins MA, Moon HK, Davis-Richardson A, Uludag M, Watson-Haigh NS, Challis R, Nakamura H, Favreau E, Gómez EA, Pluskal T, Leonard G, Rumpf W, Wurm Y (2019) Sequenceserver: A Modern Graphical User Interface for Custom BLAST Databases. Mol Biol Evol 36:2922–2924. https://doi.org/10.1093/molbev/msz185

Rao ST, Rossmann MG (1973) Comparison of super-secondary structures in proteins. J Mol Biol 76:241–256. https://doi.org/10.1016/0022-2836(73)90388-4

Rees DA, Conway E (1962) The structure and biosynthesis of porphyran: a comparison of some samples. Biochem J 84:411–416. https://doi.org/10.1042/bj0840411

Reisky L, Préchoux A, Zühlke MK, Bäumgen M, Robb CS, Gerlach N, Roret T, Stanetty C, Larocque R, Michel G, Song T, Markert S, Unfried F, Mihovilovic MD, Trautwein-Schult A, Becher D, Schweder T, Bornscheuer UT, Hehemann JH (2019) A marine bacterial enzymatic cascade degrades the algal polysaccharide ulvan. Nat Chem Biol 15:803–812. https://doi.org/10.1038/s41589-019-0311-9

Reisky L, Büchsenschütz HC, Engel J, Song T, Schweder T, Hehemann JH, Bornscheuer UT (2018) Oxidative demethylation of algal carbohydrates by cytochrome P450 monooxygenases brief-communication. Nat Chem Biol 14:342–344. https://doi.org/10.1038/s41589-018-0005-8

Robb CS, Reisky L, Bornscheuer UT, Hehemann JH (2018) Specificity and mechanism of carbohydrate demethylation by cytochrome P450 monooxygenases. Biochem J 475:3875–3886. 475:3875–3886. https://doi.org/10.1042/BCJ20180762

Salentin S, Schreiber S, Haupt VJ, Adasme MF, Schroeder M (2015) PLIP: fully automated protein-ligand interaction profiler. Nucleic Acids Res 43:W443-7. https://doi.org/10.1093/nar/gkv315

Sanghani PC, Stone CL, Ray BD, Pindel E V., Hurley TD, Bosron WF (2000) Kinetic mechanism of human glutathione-dependent formaldehyde dehydrogenase. Biochemistry 39:10720–10729. https://doi.org/10.1021/bi9929711

Shishodia S, Zhang D, El-Sagheer AH, Brown T, Claridge TDW, Schofield CJ, Hopkinson RJ (2018) NMR analyses on N-hydroxymethylated nucleobases-implications for formaldehyde toxicity and nucleic acid demethylases. Org Biomol Chem 16:4021–4032. https://doi.org/10.1039/c8ob00734a

Sichert A, Corzett CH, Schechter MS, Unfried F, Markert S, Becher D, Fernandez-Guerra A, Liebeke M, Schweder T, Polz MF, Hehemann JH (2020) Verrucomicrobia use hundreds of enzymes to digest the algal polysaccharide fucoidan. Nat Microbiol 5:1026–1039. https://doi.org/10.1038/s41564-020-0720-2

Sievers F, Wilm A, Dineen D, Gibson TJ, Karplus K, Li W, Lopez R, McWilliam H, Remmert M,

Söding J, Thompson JD, Higgins DG (2011) Fast, scalable generation of high-quality protein multiple sequence alignments using Clustal Omega. Mol Syst Biol 7:539. https://doi.org/10.1038/msb.2011.75

Sirota FL, Maurer-Stroh S, Li Z, Eisenhaber F, Eisenhaber B (2021) Functional Classification of Super-Large Families of Enzymes Based on Substrate Binding Pocket Residues for Biocatalysis and Enzyme Engineering Applications. Front Bioeng Biotechnol 9:701120. https://doi.org/10.3389/fbioe.2021.701120

Sützl L, Laurent CVFP, Abrera AT, Schütz G, Ludwig R, Haltrich D (2018) Multiplicity of enzymatic functions in the CAZy AA3 family. Appl Microbiol Biotechnol 102:2477–2492. https://doi.org/10.1007/s00253-018-8784-0

Takeda K, Matsumura H, Ishida T, Samejima M, Ohno H, Yoshida M, Igarashi K, Nakamura N (2015) Characterization of a novel PQQ-dependent quinohemoprotein pyranose dehydrogenase from *Coprinopsis cinerea* classified into auxiliary activities family 12 in carbohydrate-active enzymes. PLoS One 10: e0115722. https://doi.org/10.1371/journal.pone.0115722

Tayri-Wilk T, Slavin M, Zamel J, Blass A, Cohen S, Motzik A, Sun X, Shalev DE, Ram O, Kalisman N (2020) Mass spectrometry reveals the chemistry of formaldehyde cross-linking in structured proteins. Nat Commun 11: 3128. https://doi.org/10.1038/s41467-020-16935-w

Teeling H, Fuchs BM, Becher D, Klockow C, Gardebrecht A, Bennke CM, Kassabgy M, Huang S, Mann AJ, Waldmann J, Weber M, Klindworth A, Otto A, Lange J, Bernhardt J, Reinsch C, Hecker M, Peplies J, Bockelmann FD, Callies U, Gerdts G, Wichels A, Wiltshire KH, Glöckner FO, Schweder T, Amann R (2012) Substrate-controlled succession of marine bacterioplankton populations induced by a phytoplankton bloom. Science 336:608–611. https://doi.org/10.1126/science.1218344

Thomas F, Hehemann JH, Rebuffet E, Czjzek M, Michel G (2011a) Environmental and gut Bacteroidetes: The food connection. Front Microbiol 2:93. https://doi.org/10.3389/fmicb.2011.00093

Thomas F, Barbeyron T, Michel G (2011b) Evaluation of reference genes for real-time quantitative PCR in the marine flavobacterium *Zobellia galactanivorans*. J Microbiol Methods 84:61–66. https://doi.org/10.1016/j.mimet.2010.10.016

Trincone A (2011) Marine biocatalysts: Enzymatic features and applications. Mar Drugs 9:478–499. https://doi.org/10.3390/md9040478

Trivić S, Leskova V, Winston GW (1999) Aldehyde dismutase activity of yeast alcohol dehydrogenase. Biotechnol Lett 21:231–234. https://doi.org/10.1023/A:1005476115349

Unsworth LD, Van Der Oost J, Koutsopoulos S (2007) Hyperthermophilic enzymes - Stability, activity and implementation strategies for high temperature applications. FEBS J 274:4044–4056. https://doi.org/10.1111/j.1742-4658.2007.05954.x

Vagin A, Teplyakov A (2010) Molecular replacement with MOLREP. Acta Crystallogr D 66:22–25. https://doi.org/10.1107/S0907444909042589

Vorholt JA (2002) Cofactor-dependent pathways of formaldehyde oxidation in methylotrophic bacteria. Arch Microbiol 178:239–249. https://doi.org/10.1007/s00203-002-0450-2

Williams CJ, Headd JJ, Moriarty NW, Prisant MG, Videau LL, Deis LN, Verma V, Keedy DA, Hintze BJ, Chen VB, Jain S, Lewis SM, Arendall WB 3rd, Snoeyink J, Adams PD, Lovell SC, Richardson JS, Richardson DC (2018) MolProbity: More and better reference data for improved all-atom structure validation. Protein Sci 27:293–315. https://doi.org/10.1002/pro.3330

Willson BJ, Herman R, Langer S, Thomas GH (2022) Improved furfural tolerance in *Escherichia coli* mediated by heterologous NADH-dependent benzyl alcohol dehydrogenases. Biochem J 479:1045–1058. https://doi.org/10.1042/BCJ20210811

Yonemitsu H, Kikuchi Y (2018) Biodegradation of high concentrations of formaldehyde using *Escherichia coli* expressing the formaldehyde dismutase gene of *Methylobacterium sp*. FD1. Biosci Biotechnol Biochem 82:49–56. https://doi.org/10.1080/09168451.2017.1397497

Yurimoto H, Kato N, Sakai Y (2005) Assimilation, dissimilation, and detoxification of formaldehyde, a central metabolic intermediate of methylotrophic metabolism. Chem Rec 5:367–375. https://doi.org/10.1002/tcr.20056

Zallot R, Oberg N, Gerlt JA (2019) The EFI Web Resource for genomic enzymology tools: Leveraging Protein, Genome, and Metagenome Databases to Discover Novel enzymes and Metabolic Pathways. Biochemistry 58:4169–4182. https://doi.org/10.1021/acs.biochem.9b00735

Zhang R, Xu Y, Xiao R (2015) Redesigning alcohol dehydrogenases/reductases for more efficient biosynthesis of enantiopure isomers. Biotechnol Adv 33:1671–1684. https://doi.org/10.1016/j.biotechadv.2015.08.002

Zheng YG, Yin HH, Yu DF, Chen X, Tang XL, Zhang XJ, Xue YP, Wang YJ, Liu ZQ (2017) Recent advances in biotechnological applications of alcohol dehydrogenases. Appl Microbiol Biotechnol 101:987–1001. https://doi.org/10.1007/s00253-016-8083-6

Zhu Y, Thomas F, Larocque R, Li N, Duffieux D, Cladière L, Souchaud F, Michel G, McBride MJ (2017) Genetic analyses unravel the crucial role of a horizontally acquired alginate lyase for brown algal biomass degradation by *Zobellia galactanivorans*. Environ Microbiol 19:2164–2181. https://doi.org/10.1111/1462-2920.13699

Zobell CE (1941) Studies on marine bacteria. I. The cultural requirements of heterotrophic aerobes. J Mar Res 4:41–75.

Figure legends

Fig. 1 Porphyran contains 6-*O*-methyl-D-galactose, which can be metabolized by marine bacteria via oxidative demethylation. **a**) Porphyran, the common name of the galactan of red algae of the genus *Porphyra*, consists of chains composed mainly of the alternating monosaccharide units 4-linked-α-L-galactose-6-sulfate (L6S) and 3-linked-β-D-galactose (Gal) or 3,6-anhydro-α-L-galactose (LA). Furthermore, *O*-methylation of D-galactose results in the formation of 6-*O*-methyl-D-galactose (G6Me). **b**) The oxidative demethylation of G6Me is catalyzed by a cytochrome P450 monooxygenase in combination with its redox partners ferredoxin and ferredoxin reductase, producing D-galactose and formaldehyde in equimolar amounts. **c**) In *Formosa agariphila* KMM 3901^T and **d**) *Zobellia galactanivorans* Dsij^T, genes encoding for the key enzymes of oxidative demethylation are located in close proximity to a gene encoding for a zinc-dependent alcohol dehydrogenase. *BN863_, for example *21030 refers to locus tag *BN863_21030* for *F. agariphila* while -zgal, for example -4674 refers to locus tag *zgal_4674* for *Z. galactanivorans*.

Fig. 2 Knockout of the ADH gene in *Z. galactanivorans* leads to impaired growth on G6Me. Different *Z. galactanivorans* strains (wild type (WT), gene knockout ADH (Δ*ADH*), and gene knockout CYP (Δ*CYP*)) were incubated in minimal medium amended with D-galactose or G6Me for 3 days at RT.

Fig. 3 Thiol-dependent detoxification of formaldehyde catalyzed by an ADH and an esterase. **a**) Principle of thiol-dependent detoxification of formaldehyde and **b**) investigated thiols.

Fig. 4 Influence of pH and buffer components on the ADH activity. pH optimum for the reduction reaction of **a**) FoADH and **b**) ZoADH as well as the pH optimum for the oxidation reaction catalyzed by **d**) FoADH and **e**) ZoADH. **c**) Reduction of benzaldehyde and **f**) oxidation of benzyl alcohol by the ADHs at the respective pH optima using various buffers. A pH of 6.5 was employed for the reduction reaction and a pH of 8.5 for the oxidation reaction; all buffers had a concentration of 50 mM. Since some buffers including Bicine, Tricine, Tris, MOPSO and HEPES contain hydroxyl groups, a falsified activity due to turnover of these substances was excluded by a measurement without additional substrate. However, no activity was observed for any buffer component. All measurements (**a**-**f**) were performed under following conditions: a final substrate concentration of 10 mM benzyl alcohol or benzaldehyde, 3.5% (v/v) DMSO and 0.5 mM NAD^+ or NADH was used. The reaction was started by the addition of ADH at a final enzyme concentration of 0.1 mg mL^{-1}. The measurement was performed at 25 °C in the respective buffers with concentrations of 50 mM. The maximum relative activity (100%) corresponds to the measurements in the 50 mM NaPi buffers pH 6.5 for reduction and pH 8.5 for oxidation reactions. All measurements were performed as triplicates, the mean is given and the error bars indicate the standard deviation.

Fig. 5 Temperature optimum and thermostability of the ADHs. **a**) Influence of temperature on enzyme activity. The measurement was performed at various temperatures ranging from 20 to 80 °C for 10 min. The maximum relative activity (100%) corresponds to the measurement at 75 °C for both enzymes. Influence of temperature on enzyme stability for **b**) FoADH and **c**) ZoADH. The enzymes with a concentration of 1 mg mL^{-1} were incubated at different temperatures between 20 and 80 °C for 1 or 4 hours, followed by the determination of residual activity. The measurement was performed at 40 °C. The maximum relative activity (100%) corresponds to a control incubated on ice for 1 or 4 h. All measurements (**a**-**c**) were performed under following conditions: a final substrate concentration of 10 mM benzyl alcohol and 0.5 mM

NAD$^+$ was used. The reaction was started by the addition of ADH at a final enzyme concentration of 0.1 mg mL^{-1}. The measurements were performed in a 50 mM NaPi buffer pH 7.5. All measurements were performed as triplicates, the mean is given and the error bars indicate the standard deviation.

Fig. 6 Crystal structures of FoADH and ZoADH. **a**) Monomer structures of ZoADH and FoADH. Catalytic and cofactor domain are indicated by cyan and green, respectively. NAD$^+$ and zinc ions are indicated by yellow stick and grey sphere, respectively. **b**) Superimposition of closed (green) and open conformation between catalytic and cofactor-binding domains of ZoADH and FoADH monomers. The superimposed cofactor-binding domain of ZoADH and FoADH are indicated as grey cartoon. **c**) Tetrameric formation of ZoADH and FoADH. **d**) Superimposition of tetrameric formation of FoADH (green) and ZoADH (cyan). **e**) Superimposition of monomer structure of FoADH (green) and ZoADH (cyan) with all-trans-retinol dehydrogenase ADH4 from *Homo sapiens* (pink, PDB code: 3COS), uncharacterized zinc-type alcohol dehydrogenase-like protein YdjJ from *E. coli* (wheat, 5vm2), scyllo-inosose 3-dehydrogenase from *Thermotoga maritima* (3IP1, yellow).

Fig. 7 Active sites of FoADH and ZoADH. **a**) Interaction of ZoADH and FoADH with NAD$^+$ and zinc ion at the Zn1 site. **b**) Superimposition of active site of open and closed conformation of FoADH and ZoADH. **c**) Comparison of electrostatic surface structure of open and closed conformations of FoADH and ZoADH

Figures

Fig. 1

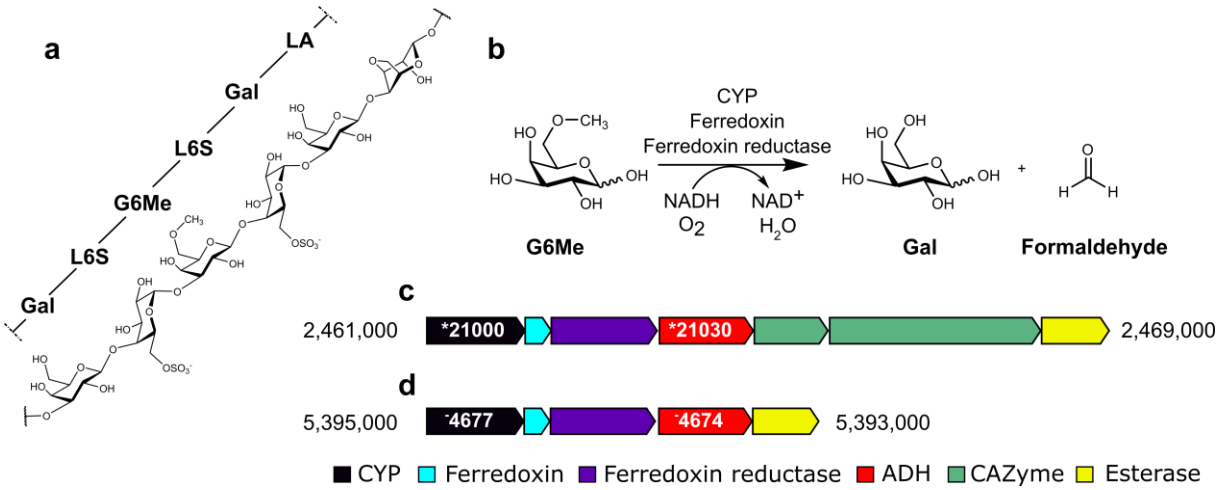

Fig. 2

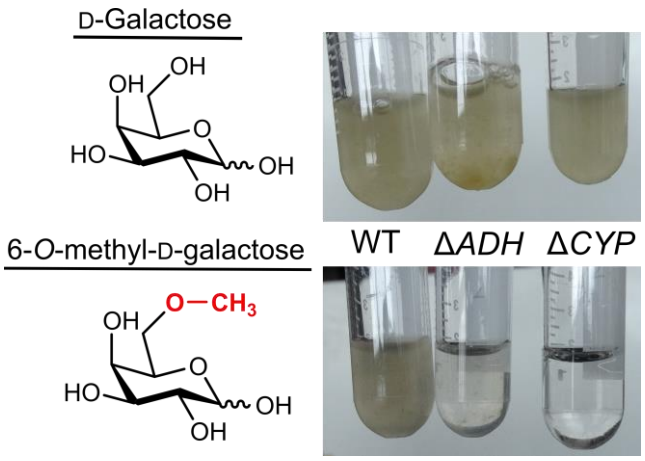
D-Galactose
OH
OH
O
HO
OH
OH
6-O-methyl-D-galactose
O—CH3
OH
O
HO
OH
OH
WT
ΔADH
ΔCYP

Fig. 3

a

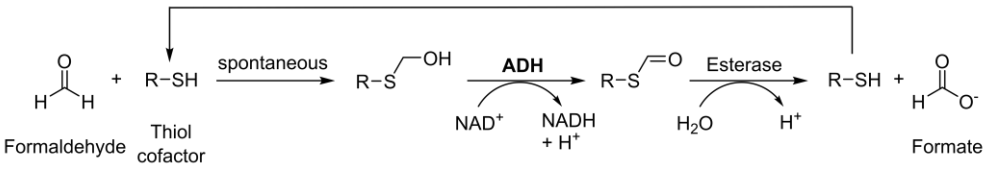
Formaldehyde
Thiol cofactor
spontaneous
ADH
NAD+
NADH + H+
Esterase
H2O
H+
Formate

b

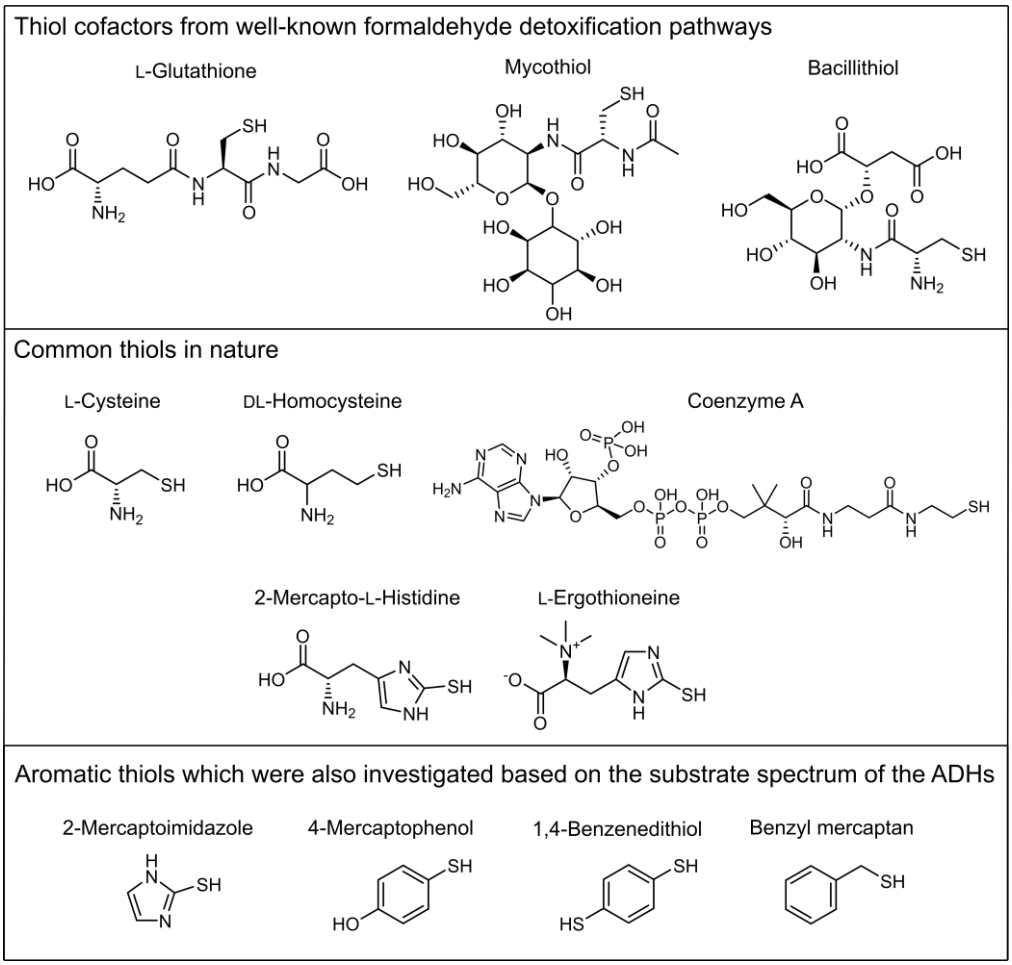
Thiol cofactors from well-known formaldehyde detoxification pathways
L-Glutathione
Mycothiol
Bacillithiol
Common thiols in nature
L-Cysteine
DL-Homocysteine
Coenzyme A
2-Mercapto-L-Histidine
L-Ergothioneine
Aromatic thiols which were also investigated based on the substrate spectrum of the ADHs
2-Mercaptoimidazole
4-Mercaptophenol
1,4-Benzenedithiol
Benzyl mercaptan

Fig. 4

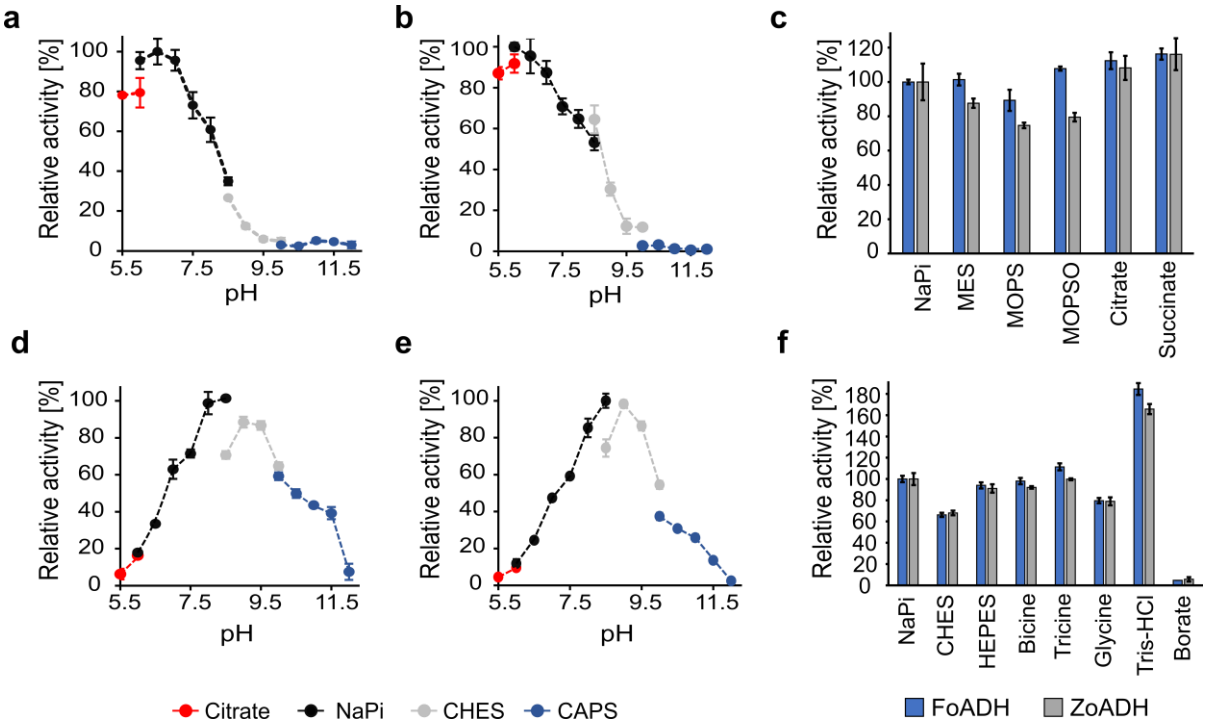
a
b
c
d
e
f
Relative activity [%]
pH
5.5
7.5
9.5
11.5
NaPi
MES
MOPS
MOPSO
Citrate
Succinate
CHES
HEPES
Bicine
Tricine
Glycine
Tris-HCl
Borate
Citrate
NaPi
CHES
CAPS
FoADH
ZoADH

Fig. 5

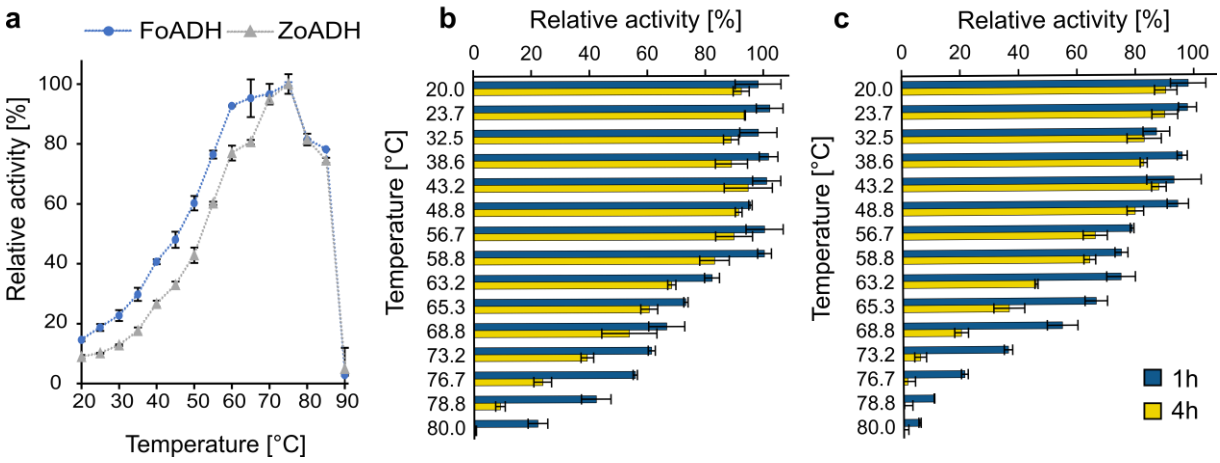
a
FoADH
ZoADH
Relative activity [%]
Temperature [°C]
b
Relative activity [%]
Temperature [°C]
c
Relative activity [%]
Temperature [°C]
1h
4h

Fig. 6

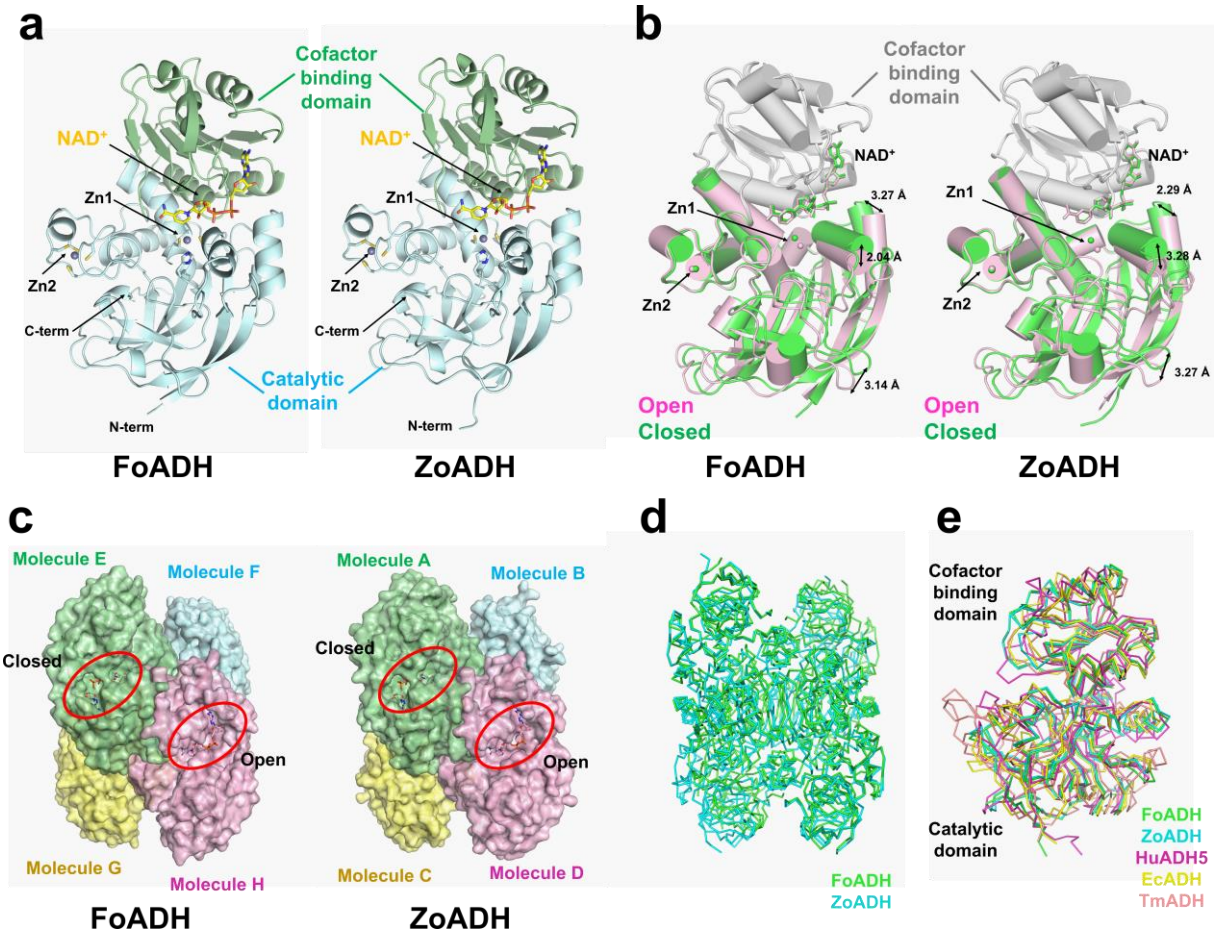
a
Cofactor binding domain
NAD+
Zn1
Zn2
C-term
Catalytic domain
N-term
FoADH
ZoADH
b
Cofactor binding domain
NAD+
Zn1
Zn2
3.27 Å
2.04 Å
3.14 Å
2.29 Å
3.28 Å
3.27 Å
Open
Closed
FoADH
ZoADH
c
Molecule E
Molecule F
Molecule G
Molecule H
Molecule A
Molecule B
Molecule C
Molecule D
Closed
Open
FoADH
ZoADH
d
FoADH
ZoADH
e
Cofactor binding domain
Catalytic domain
FoADH
ZoADH
HuADH5
EcADH
TmADH

Fig. 7

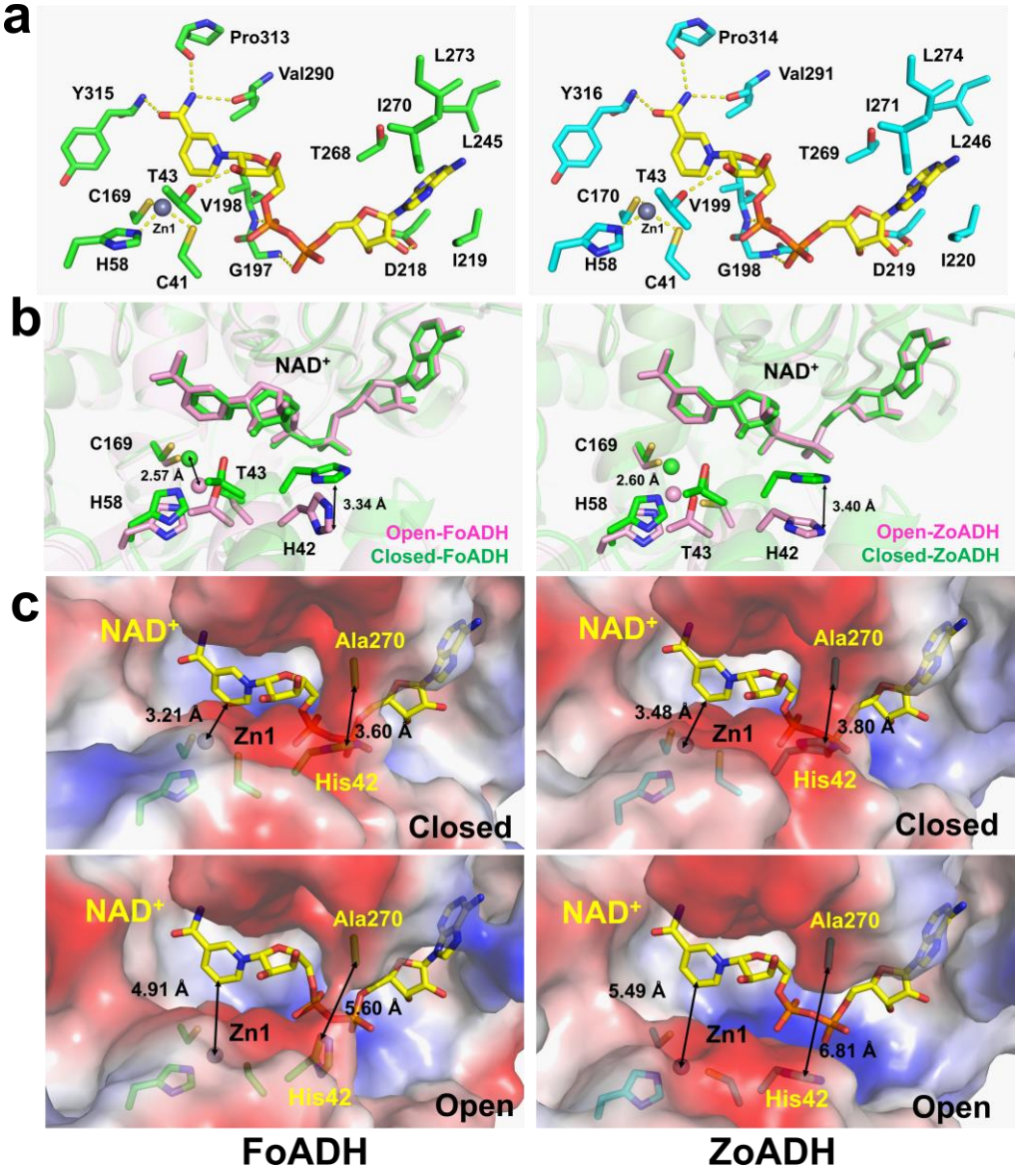
a
Pro313
Val290
L273
Y315
I270
L245
T268
T43
C169
V198
Zn1
H58
C41
G197
D218
I219
Pro314
Val291
L274
Y316
I271
L246
T269
T43
C170
V199
Zn1
H58
C41
G198
D219
I220
b
NAD+
C169
2.57 Å
T43
H58
3.34 Å
H42
Open-FoADH
Closed-FoADH
NAD+
C169
2.60 Å
H58
3.40 Å
T43
H42
Open-ZoADH
Closed-ZoADH
c
NAD+
Ala270
3.21 Å
Zn1
3.60 Å
His42
Closed
NAD+
Ala270
3.48 Å
Zn1
3.80 Å
His42
Closed
NAD+
Ala270
4.91 Å
Zn1
5.60 Å
His42
Open
NAD+
Ala270
5.49 Å
Zn1
6.81 Å
His42
Open
FoADH
ZoADH

Tables

Table 1 Initial substrate screening of the ADH in the reduction direction revealed that they preferentially convert aromatic aldehydes. Substrates were employed at a final concentration of 10 mM. For NADH a concentration of 0.5 mM was used. The reaction contained 3.5% (v/v) DMSO. The reaction was conducted in a 50 mM succinate buffer pH 6.5 at an incubation temperature of 70 °C. All measurements were performed as triplicates, the mean and the standard deviation is given.

Abbr.	Substrates	Specific activity [U/mg]	
		FoADH	ZoADH
1	Pyridine-3-carbaldehyde	64.09 ± 2.39	54.85 ± 4.34
2	Furfural	47.77 ± 1.19	44.78 ± 2.07
3	5-(Hydroxymethyl)furfural	44.81 ± 2.16	38.29 ± 2.47
4	Thiophene-3-carbaldehyde	37.45 ± 4.19	29.32 ± 2.59
5	Terephthalaldehyde	30.05 ± 3.60	27.34 ± 4.68
6	Isophthalaldehyde	26.71 ± 1.47	36.94 ± 3.68
7	Phthalaldehyde	n.d.[a)]	n.d.
8	Hydrocinnamaldehyde	26.00 ± 2.23	30.13 ± 2.32
9	Cinnamaldehyde[b)]	12.57 ± 0.90	11.20 ± 0.11
10	Phenylacetaldehyde	n.d.	n.d.
11	Phenylglyoxal	n.d.	n.d.
12	Benzaldehyde	5.14 ± 0.09	12.49 ± 0.73
13	*m*-Tolualdehyde	6.30 ± 1.06	7.32 ± 0.32
14	*p*-Tolualdehyde	4.71 ± 0.32	5.60 ± 0.44
15	*o*-Tolualdehyde	0.04 ± 0.01	0.04 ± 0.01
16	Acetophenone	n.d.	n.d.
17	Benzoylacetone	n.d.	n.d.
18	Formaldehyde	n.d.	n.d.
19	Propionaldehyde	1.58 ± 0.10	0.92 ± 0.36
20	Butyraldehyde	3.62 ± 1.04	4.02 ± 0.48
21	Caproaldehyde	7.07 ± 0.64	6.62 ± 0.30

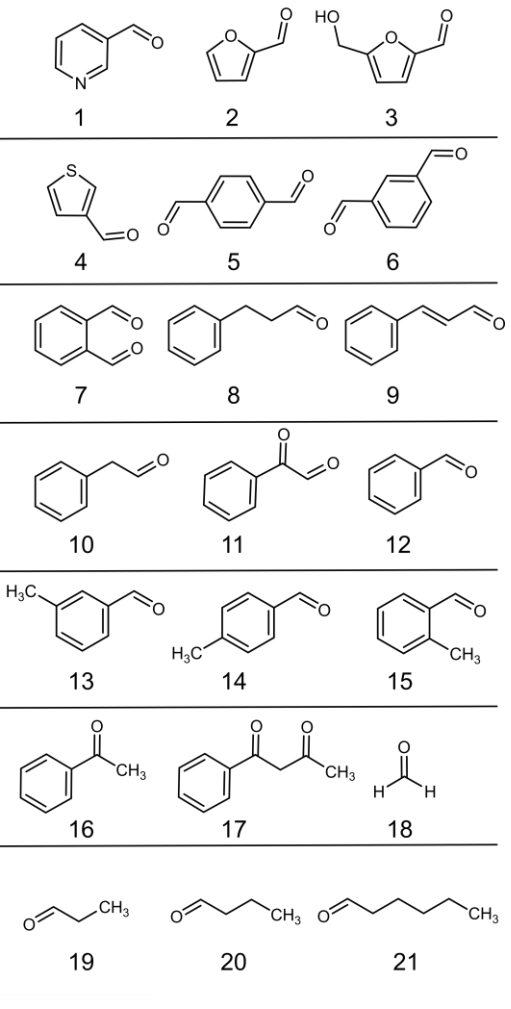

a) n.d.: not detected

b) Due to a high background absorption of the component, a substrate concentration of 1mM was employed.

Table 2 Both ADHs possess minor specific activities for the oxidation of alcohols. Formaldehyde was also tested in a possible oxidation reaction to exclude thiol-independent formaldehyde dehydrogenase activity. Substrates were employed at a final concentration of 10 mM. For NAD^+ a concentration of 0.5 mM was used. The reaction contained 3.5% (v/v) DMSO. The reaction was conducted in a 50 mM NaPi buffer pH 8.5 at an incubation temperature of 70 °C. All measurements were performed as triplicates, the mean and the standard deviation is given.

Abbr.	Substrate	Specific activity [mU/mg] FoADH	Specific activity [mU/mg] ZoADH
1	2,5-Bis(hydroxymethyl)furan	490 ± 50	290 ± 90
2	Furfuryl alcohol	310 ± 10	194 ± 51
3	5-(Hydroxymethyl)furfural	n.d.[a)]	n.d.
4	5-(Hydroxymethyl)furan-2-carboxylic acid	n.d.	n.d.
5	3,4-Bis(hydroxymethyl)furan	n.d.	n.d.
6	1,4-Benzenedimethanol	86 ± 1.5	51 ± 3.0
7	Benzyl alcohol	81 ± 0.7	53 ± 0.1
8	Cinnamyl alcohol[b)]	11 ± 3.1	6 ± 2.9
9	Methanol	n.d.	n.d.
10	Ethanol	n.d.	n.d.
11	Formaldehyde	n.d.	n.d.

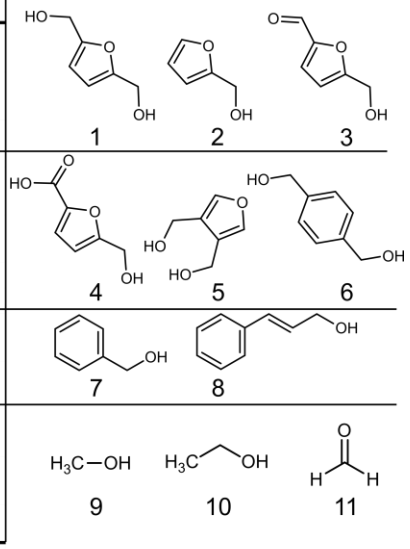

a) n.d.: not detected

b) Due to a high background absorption of the component, a substrate concentration of 1mM was employed.

Table 3 Influence of various substances on the enzyme activity of both ADHs. The ADH was incubated with the respective component for 1 h at RT prior to measurement. The maximum relative activity (100%) corresponds to the measurement for the control, which contained no additives. All measurements were performed under following conditions: a final substrate concentration of 10 mM benzyl alcohol and 0.5 mM NAD^+ was used. The reaction was started by the addition of ADH at a final enzyme concentration of 0.1 mg mL^{-1}. The measurements were performed in a 50 mM HEPES buffer pH 8.5 at 25 °C. All measurements were performed as triplicates, the mean and the standard deviation is given.

Chemical	Conc. [mM]	Relative activity [%]	
		FoADH	ZoADH
None	-	100 ± 1.3	100 ± 9.3
KCl	10	121 ± 1.9	154 ± 7.9
$CaCl_2$	10	188 ± 6.3	306 ± 9.9
$MgCl_2$	10	219 ± 7.2	328 ± 11.7
$NiCl_2$	10	891 ± 13.8	1004 ± 6.6
$CoCl_2$	10	1280 ± 38.1	1242 ± 25.4
$MnCl_2$	10	1394 ± 58.5	973 ± 45.0
$ZnCl_2$	10	n.d.[a)]	n.d.
$CuCl_2$	10	n.d.	n.d.
$FeCl_3$	10	n.d.	n.d.
EDTA	25	61 ± 1.9	61 ± 7.8
DTT	10	48 ± 4.6	85 ± 3.9
2-ME	10	19 ± 1.7	28 ± 4.1

a) n.d.: not detected

Tables

Table 1 Initial substrate screening of the ADH in the reduction direction revealed that they preferentially convert aromatic aldehydes. Substrates were employed at a final concentration of 10 mM. For NADH a concentration of 0.5 mM was used. The reaction contained 3.5% (v/v) DMSO. The reaction was conducted in a 50 mM succinate buffer pH 6.5 at an incubation temperature of 70 °C. All measurements were performed as triplicates, the mean and the standard deviation is given.

Abbr.	Substrates	Specific activity [U/mg]	
		FoADH	ZoADH
1	Pyridine-3-carbaldehyde	64.09 ± 2.39	54.85 ± 4.34
2	Furfural	47.77 ± 1.19	44.78 ± 2.07
3	5-(Hydroxymethyl)furfural	44.81 ± 2.16	38.29 ± 2.47
4	Thiophene-3-carbaldehyde	37.45 ± 4.19	29.32 ± 2.59
5	Terephthalaldehyde	30.05 ± 3.60	27.34 ± 4.68
6	Isophthalaldehyde	26.71 ± 1.47	36.94 ± 3.68
7	Phthalaldehyde	n.d.[a)]	n.d.
8	Hydrocinnamaldehyde	26.00 ± 2.23	30.13 ± 2.32
9	Cinnamaldehyde[b)]	12.57 ± 0.90	11.20 ± 0.11
10	Phenylacetaldehyde	n.d.	n.d.
11	Phenylglyoxal	n.d.	n.d.
12	Benzaldehyde	5.14 ± 0.09	12.49 ± 0.73
13	*m*-Tolualdehyde	6.30 ± 1.06	7.32 ± 0.32
14	*p*-Tolualdehyde	4.71 ± 0.32	5.60 ± 0.44
15	*o*-Tolualdehyde	0.04 ± 0.01	0.04 ± 0.01
16	Acetophenone	n.d.	n.d.
17	Benzoylacetone	n.d.	n.d.
18	Formaldehyde	n.d.	n.d.
19	Propionaldehyde	1.58 ± 0.10	0.92 ± 0.36
20	Butyraldehyde	3.62 ± 1.04	4.02 ± 0.48
21	Caproaldehyde	7.07 ± 0.64	6.62 ± 0.30

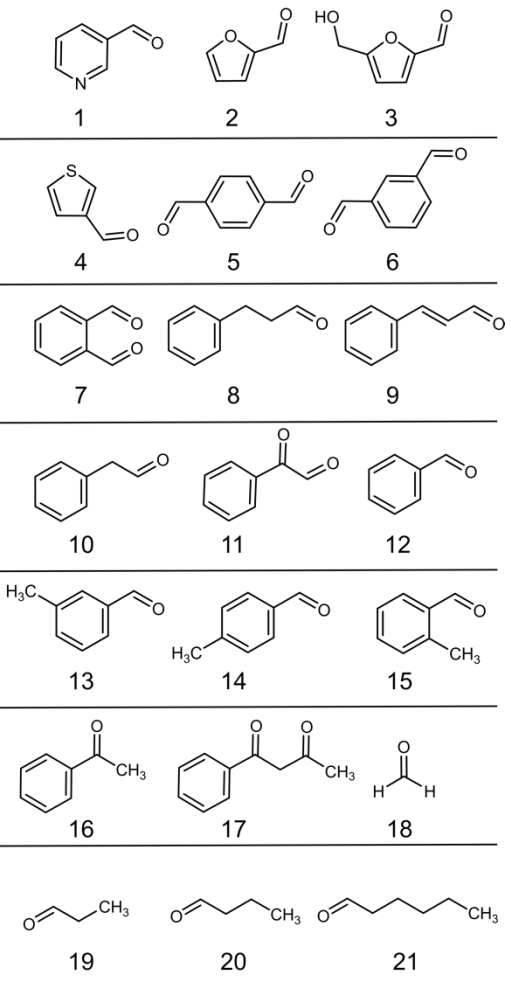

a) n.d.: not detected

b) Due to a high background absorption of the component, a substrate concentration of 1mM was employed.

Table 2 Both ADHs possess minor specific activities for the oxidation of alcohols. Formaldehyde was also tested in a possible oxidation reaction to exclude thiol-independent formaldehyde dehydrogenase activity. Substrates were employed at a final concentration of 10 mM. For NAD^+ a concentration of 0.5 mM was used. The reaction contained 3.5% (v/v) DMSO. The reaction was conducted in a 50 mM NaPi buffer pH 8.5 at an incubation temperature of 70 °C. All measurements were performed as triplicates, the mean and the standard deviation is given.

Abbr.	Substrate	Specific activity [mU/mg] FoADH	Specific activity [mU/mg] ZoADH
1	2,5-Bis(hydroxymethyl)furan	490 ± 50	290 ± 90
2	Furfuryl alcohol	310 ± 10	194 ± 51
3	5-(Hydroxymethyl)furfural	n.d.[a)]	n.d.
4	5-(Hydroxymethyl)furan-2-carboxylic acid	n.d.	n.d.
5	3,4-Bis(hydroxymethyl)furan	n.d.	n.d.
6	1,4-Benzenedimethanol	86 ± 1.5	51 ± 3.0
7	Benzyl alcohol	81 ± 0.7	53 ± 0.1
8	Cinnamyl alcohol[b)]	11 ± 3.1	6 ± 2.9
9	Methanol	n.d.	n.d.
10	Ethanol	n.d.	n.d.
11	Formaldehyde	n.d.	n.d.

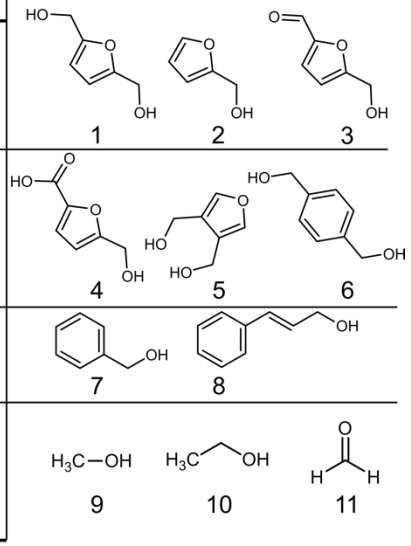

a) n.d.: not detected

b) Due to a high background absorption of the component, a substrate concentration of 1mM was employed.

Table 3 Influence of various substances on the enzyme activity of both ADHs. The ADH was incubated with the respective component for 1 h at RT prior to measurement. The maximum relative activity (100%) corresponds to the measurement for the control, which contained no additives. All measurements were performed under following conditions: a final substrate concentration of 10 mM benzyl alcohol and 0.5 mM NAD^+ was used. The reaction was started by the addition of ADH at a final enzyme concentration of 0.1 mg mL^{-1}. The measurements were performed in a 50 mM HEPES buffer pH 8.5 at 25 °C. All measurements were performed as triplicates, the mean and the standard deviation is given.

Chemical	Conc. [mM]	Relative activity [%]	
		FoADH	ZoADH
None	-	100 ± 1.3	100 ± 9.3
KCl	10	121 ± 1.9	154 ± 7.9
$CaCl_2$	10	188 ± 6.3	306 ± 9.9
$MgCl_2$	10	219 ± 7.2	328 ± 11.7
$NiCl_2$	10	891 ± 13.8	1004 ± 6.6
$CoCl_2$	10	1280 ± 38.1	1242 ± 25.4
$MnCl_2$	10	1394 ± 58.5	973 ± 45.0
$ZnCl_2$	10	n.d.[a)]	n.d.
$CuCl_2$	10	n.d.	n.d.
$FeCl_3$	10	n.d.	n.d.
EDTA	25	61 ± 1.9	61 ± 7.8
DTT	10	48 ± 4.6	85 ± 3.9
2-ME	10	19 ± 1.7	28 ± 4.1

a) n.d.: not detected